Spring 2-1-2018

GLOBAL SEAWATER REDOX TRENDS DURING THE LATE DEVONIAN MASS EXTINCTION DETECTED USING U ISOTOPES OF MARINE CARBONATES

David Allen White
University of New Mexico

David White

Candidate

Earth and Planetary Sciences

Department

This thesis is approved, and it is acceptable in quality and form for publication:

Approved by the Thesis Committee:

Dr. Maya Elrick, Earth and Planetary Sciences, Chairperson

Dr. Viorel Atudorei, Earth and Planetary Sciences

Dr. Peter Fawcett, Earth and Planetary Sciences

Dr. Stephen Romaniello, Arizona State University

GLOBAL SEAWATER REDOX TRENDS DURING THE LATE DEVONIAN MASS EXTINCTION DETECTED USING U ISOTOPES OF MARINE CARBONATES

by

DAVID WHITE

B.S., GEOLOGY, UNIVERSITY OF TENNESSEE, 2014

THESIS

Submitted in Partial Fulfillment of the
Requirements for the Degree of

Master of Science

Earth and Planetary Sciences

The University of New Mexico
Albuquerque, New Mexico

May 2018

ACKNOWLEDGEMENTS

I would like to thank my committee chair, Dr. Maya Elrick, for her tireless commitment to this project and her exceptional guidance throughout my years of graduate study. I also thank my committee members, Dr. Viorel Atudorei, Dr. Peter Fawcett, and Dr. Stephen Romaniello who provided excellent support to both myself and this project.

This research was partially funded by the Geological Society of America, University of New Mexico Earth and Planetary Sciences Department, the University of New Mexico Graduate and Professional Student Association, and the National Science Foundation (Elrick #17-536). I thank you for your generous support and funding to this project.

Many thanks for field assistance by Dios Salas da Costa, long discussions and advice from Rickey Bartlett and Remy Rovelli, and initial geochemical analysis by Dr. Troy Rasbury (Stony Brook). Finally, I thank my wife, Rachel, for all the support, encouragement, and inspiration she has given me over the years.

GLOBAL SEAWATER REDOX TRENDS DURING THE LATE DEVONIAN MASS EXTINCTION DETECTED USING U ISOTOPES OF MARINE CARBONATES

by

David White

B.S., Geology, University of Tennessee, 2014

M.S., Geology, University of New Mexico, 2018

ABSTRACT

The Late Devonian extinction ranks as one of the 'big five' Phanerozoic extinctions affecting up to 80% of marine species and occurred during five distinct pulses spanning <3 My. The leading hypotheses explaining the pulsed extinctions are global cooling and/or widespread marine anoxia. We test the marine anoxia hypothesis by analyzing uranium isotopes ($\delta^{238}U$) across a ~7 My interval of well-dated Upper Devonian marine carbonates from the Devil's Gate Limestone in Nevada, USA.

The measured $\delta^{238}U$ curve shows no co-variation with local anoxic facies, water-depth dependent facies changes, redox-sensitive metals, TOC, or diagnostic elemental ratios indicating the $\delta^{238}U$ curve was not controlled by local depositional or diagenetic processes and represents global seawater redox conditions. Two negative $\delta^{238}U$ shifts (indicating more reducing seawater) are observed with durations of ~3.8 My (late Frasnian) and ~1.1 My (early Famennian), respectively.

Steady-state modeling of the observed -0.2 to -0.3‰ shifts in $\delta^{238}U$ points to a ~5-15% increase in the total area of anoxic seafloor during these excursions. The late Frasnian negative shift is broadly coincident with the first extinction pulse (late *rhenana* Zone or lower Kellwasser event), whereas the early Famennian negative shift (lower-middle *triangularis* zones) does not coincide with the most intense Frasnian-Famennian boundary (F-F) extinction pulses (upper Kellwasser event). Compilations of local sediment redox conditions from Upper Devonian marine deposits with conodont zone-level age control indicates that the extinction pulses were coincident with widespread anoxic deposits accumulating in subtropical epeiric sea and some open-ocean settings supporting previous interpretations that widespread marine anoxia had an important influence on the Late Devonian extinction. The temporal relationships between global ocean redox trends represented by the $\delta^{238}U$ curve and the newly compiled subtropical marine redox sediment trends indicates Late Devonian global oceans and epeiric seas were in relatively good redox communication for the majority of the study interval except for a brief interval (<500 ky) spanning the F-F boundary.

TABLE OF CONTENTS

1.0 INTRODUCTION

The Late Devonian extinction ranks as one of the 'big five' Phanerozoic faunal crises with over 80% of benthic, planktonic, and nektonic marine species affected with terrestrial plants and animals influenced as well (McGhee, 1996, 2001; Hallam and Wignall, 1997; Racki, 2005; Bond and Grasby, 2016). The leading hypotheses explaining the extinction involve two brief, global cooling pulses occurring during an overall long-term warming trend (Copper, 1986; Joachimski and Buggisch, 2002) and/or widespread ocean anoxia generated by increased nutrient flux and resultant enhanced productivity and dissolved oxygen demands (Algeo et al., 1995; Algeo and Scheckler, 1998).

To test the influence of marine anoxia driving the Late Devonian extinction, we utilize U isotopes from marine carbonates to evaluate globally integrated ocean redox trends. Unlike traditional marine redox proxies, such as the occurrence of typical anoxic marine facies, framboidal pyrite size, distribution, $\delta^{34}S_{pyrite}$, and redox sensitive trace metal (RSM) abundances, which are sensitive to local depositional conditions, U isotopes of marine carbonates can provide a globally-integrated estimate of ocean redox conditions. U isotopes are sensitive to marine redox conditions because the reduction of soluble U(VI) to insoluble U(IV), which is sequestered into anoxic sediments, is associated with a large isotope fractionation (Weyer et al., 2008). This signal propagates globally because the ocean residence time of U (~400 ky; Ku et al., 1977) is significantly longer than ocean mixing times (<1 ky), and thus open-ocean seawater and the carbonates, which precipitate from

seawater, should record a homogenous U-isotope value representative of globally-averaged ocean redox conditions. The utility of U isotopes as a global-ocean redox proxy is documented by previous studies from the Neoproterozoic through Cenozoic (Montoya-Pino et al., 2010; Brennecka et al., 2011; Dahl et al., 2014; Hood et al., 2016; Lau et al., 2016; Lau et al., 2017; Elrick et al., 2017, Song et al., 2017). The specific objectives of this study are to 1) describe and interpret Late Devonian U- isotopic and trace element trends, and 2) discuss relationships among U-isotope trends, extinction records, and global and epeiric sea redox records.

2.0 BACKGROUND

2.1 Late Devonian extinction, paleogeography, and paleoclimate

The five distinct Late Devonian extinction pulses occur in the late Frasnian (*rhenana* conodont Zone often termed the lower Kellwasser event; LKW) followed by four extinctions clustered near the Frasnian-Famennian (F-F) boundary (upper Kellwasser event; UKW) (Fig. 1; Hallam and Wignall, 1997; McGhee, 1996, 2001; Bond and Grasby, 2016). In the marine realm, benthic, planktonic, and nektonic organisms were all affected with tropical stromatoporid-coral reef ecosystems particularly devastated (Copper, 2002; Kiessling et al., 2000; Kiessling and Simpson, 2011). Recent studies have suggested that this biocrisis was a function of reduced speciation rather than elevated extinction rates (Sepkoski, 1996; Bambach et al., 2004; Stigall, 2010). Nevertheless, biodiversity loss patterns indicate that 1) low-latitude regions experienced greater loss than higher-latitudes, 2) surviving groups experienced post-extinction latitudinal compression, and 3) shallow-water marine

benthic organisms experienced more severe losses than deep-water organisms. Coincident with the extinction pulses is the occurrence of widespread organic-rich marine facies (including the German organic-rich Kellwasser deposits) which was used to suggest that marine anoxia controlled extinction trends (e.g. Goodfellow et al., 1989; Buggisch, 1991; Joachimski and Buggisch, 1993).

Late Devonian global paleogeography is characterized by Laurentia straddling the paleoequator and separated from Gondwana by the narrow and closing Rheic ocean (Fig. S1). Globally high sea levels resulted in extensive continental flooding and the development of vast epeiric seas that comprised ~15% of the global ocean seafloor area. The Devonian climate records a transition from long-term greenhouse to an icehouse with oxygen isotopic evidence for glacio-eustasy occurring as early as the Middle Devonian (Elrick et al., 2009, Elrick and Witzke, 2016) and glacial tillites accumulating in South America by the Famennian (Caputo, 1985, 2008; Frakes et al., 2005; Isaacson et al., 2008).

The westward-deepening continental margin of western Laurentia accumulated up to 7.5 km of Proterozoic through Upper Devonian siliciclastic and carbonate passive-margin deposits. In the Late Devonian, convergence related to the Antler orogeny along western Laurentia resulted in the development of a foreland basin and forebulge atop the passive-margin succession (Giles and Dickenson, 1995; Morrow and Sandberg, 2008). In the central Nevada study area (Devil's Gate section), the transition between passive- and convergent-margin tectonics includes deposition of the Upper Devonian upper member of the Devil's

Gate Limestone which accumulated in slope, and outer and middle ramp environments (Table S1). At this location, the Devil's Gate Limestone has excellent age control through detailed conodont biostratigraphy (Sandberg and Poole, 1977; Sandberg et al., 1988; 2003) and established $\delta^{13}C$ trends (Joachimski et al., 2002). Six depositional facies are recognized in the ~140 m-thick studied succession and they stack to form six My-scale depositional sequences (each ~15-30 m thick). Conodont biozone age control combined with inter- and intracontinental correlations document that three of the sequences correspond to My-scale eustatic sea-level cycles termed T-R cycles IId-2, IId-3, and IIe by Johnson et al. (1985) and Morrow and Sandberg (2008) (Fig. 1).

In the study area, the upper Devil's Gate Limestone is dominated by hemi-pelagic lime mudstone and siliciclastic mudstone interbedded with outer ramp- and slope-derived carbonate debris-flow conglomerates (Fig. 1; Table S1). Although these deposits accumulated in suboxic/oxic through anoxic predominately deep-water environments, the detrital lime mud was originally generated in oxic shallow-water environments and transported downslope (along with fine siliciclastic grains) by gravity-flow processes. An original shallow-water origin (deposited in <few tens of meters) for the lime mud is particularly important for this study because geochemical analysis of the carbonate fraction is interpreted to reflect prevailing surface seawater conditions rather than deeper water conditions along the outer ramp and slope.

2.2 U-isotope systematics

Weathering of the continental crust represents the primary source of U to the global ocean and the main sinks are suboxic and anoxic continental margin sediments, altered oceanic crust, and biogenic carbonates (Morford and Emerson, 1999; Tissot and Dauphas, 2015). In oxidizing marine waters, U primarily occurs as U(VI) in the uranyl ion (UO_2^{2+}) which readily forms soluble carbonate complexes (Weyer et al., 2008). Under anoxic conditions, U(VI) is microbially reduced to relatively insoluble U(IV) and is sequestered into anoxic sediments (Klinkhammer and Palmer, 1991; Morford and Emerson, 1999). There are three naturally occurring U isotopes: ^{238}U (~99.3%), ^{235}U (~0.7%), and ^{234}U (~0.005%). During reduction of U(VI) to U(IV), U isotopes are fractionated due to the nuclear field shift effect (Bigeleisen, 1996) with ^{238}U preferentially incorporated into the reduced species (Weyer et al., 2008; Stylo et al., 2015). Because the ocean residence time of U is significantly longer than ocean mixing times (<1 ky), the U isotopic composition of seawater is uniform throughout the oceans, therefore limestones precipitated from oxic surface seawaters (<~100 meters) can track global seawater redox conditions (e.g. Brennecka et al., 2011; Dahl et al., 2014; Lau et al., 2016; Elrick et al., 2017). During intervals of increased anoxic sediment accumulation, seawater $^{238}U/^{235}U$ ratios decrease due to sequestration of ^{238}U into anoxic sediments. Carbonate minerals precipitated from seawater can record changes in the seawater $^{238}U/^{235}U$. U isotopes are reported in standard delta notation:

$$\delta^{238}U\ (‰) = [(^{238}U/^{235}U_{sample})/(^{238}U/^{235}U_{standard})-1] \times 1000$$

where the standard is CRM-112A, which has a $^{238}U/^{235}U$ ratio of 137.832 ± 0.026 (Cheng et al., 2013).

3.0 METHODS

In the study area, the upper member of the Devil's Gate Limestone was described and sampled within a sequence stratigraphic framework (Fig. 1). Samples were collected every 1-5 m spanning ~7 My of the Late Devonian (late *hassi* through *crepida* conodont zones). Samples were powdered from bulk limestone chips free of secondary calcite veins and leached in 10% HCl for ~10 minutes to remove surface contaminants. To evaluate potential isotopic differences between primary skeletal calcite versus coeval bulk carbonate values, a low Mg-calcite rugose coral fragment was analyzed and compared to its host bulk carbonate.

For $\delta^{238}U$ analysis, ~1.5 g of sample powder was digested by adding 20 mL of 1M HNO_3 followed by the slow addition of 3 mL of concentrated HNO_3 to replace spent acid. The 1M HNO_3 concentration was used to avoid the dissolution of non-carbonate material and contamination by detrital phases (i.e. organic matter, clay minerals). Following digestion, samples were centrifuged to separate the supernatant from insoluble residues, treated with a solution of 0.3 mL 32% H_2O_2 and 2 mL concentrated HNO_3, and fluxed at ~100 °C for one hour to drive off residual organic matter. After a final dry down, the samples were dissolved in a solution of 3M HNO_3 in preparation for column chemistry.

Major and trace element concentrations were determined from sample aliquots to prepare sample solutions containing at least 250 ng U to be spiked with

^{233}U-^{236}U double spike (IRMM-3636, Verbruggen et al., 2008). Addition of the ^{233}U-^{236}U double spike was performed to correct for isotope fractionation during sample preparation and instrumental mass bias. Spiked samples underwent column chemistry to isolate and collect U following the UTEVA resin method of Weyer et al. (2008). Collected U samples were treated with a solution of 32% H_2O_2 and concentrated HNO_3 twice after column chemistry to remove any organic material contaminants from the UTEVA resin then measured for their U-isotopic values and final U concentrations on a Thermo Neptune MC-ICP-MS at Arizona State University (W.M. Keck Foundation Laboratory for Environmental Biogeochemistry).

Samples were measured for their whole-rock elemental content to characterize local redox signals (via redox-sensitive trace metals and Mn/Sr ratios), detrital input (Al, K), and potential dolomitization (Mg/Ca ratios). For whole-rock analysis, 1 M HCl was added to approximately 1 g of powdered bulk limestone until no further reaction was observed. Samples were then centrifuged and the supernatant collected. Concentrated HNO_3 (35 mL) and HF (9 mL) was added to the remaining insoluble residue and fluxed at ~80 °C for >24 hours. Samples were then dried down and further dissolved with concentrated HNO_3 (10 mL) and HCl (10 mL) until all material was in solution. Samples were then recombined with their carbonate fraction solutes, dried down, and dissolved in 2% HNO_3 for ICP-MS analysis at the UNM Earth & Planetary Science Analytical Geochemistry Lab.

For total organic carbon (TOC) analysis, ~4 mg of sample powder was placed in silver capsules and placed in an evaporative 10% HCl acid wash for >24 hours.

Additional volumes of 5% HCl were added until no reaction was observed. Samples were then dried down and analyzed for their TOC content and carbon isotope ratios with a Costech ECS 4010 Elemental Analyzer coupled to a Thermo Finnigan Delta Plus mass spectrometer at the UNM Center for Stable Isotopes. To evaluate any influences of detrital input, weight percent (wt%) insoluble residues were determined. Approximately 1.5 g of sample was digested with 1M HCl until no reaction was observed, insoluble residues filtered, dried down, and reweighed.

Carbon and oxygen isotope ratios were determined using the method described by Spotl and Vennemann (2003). Approximately 0.5 mg of sample was loaded in 12 mL borosilicate tubes, flushed with He, then reacted for 12 hours with H_3PO_4 at 50 °C. Carbon and oxygen isotope measurements of the evolved CO_2 were made by continuous flow Isotope Ratio Mass Spectrometry using a Gasbench device coupled to a Thermo Fisher Scientific Delta V Plus Isotope Mass Spectrometer at the UNM Center for Stable Isotopes. Results are reported using the standard delta notation, versus V-PDB. Based on measurements of a laboratory standard (Carrara Marble), reproducibility for $\delta^{13}C$ and $\delta^{18}O$ was better than 0.1‰ for all but five samples, whose SD values range from 0.1‰ to 0.27‰. The laboratory standard was calibrated versus NBS 19, for which the $\delta^{13}C$ is 1.95‰ and $\delta^{18}O$ is -2.2‰.

4.0 RESULTS

4.1 U-isotopes

Measured $\delta^{238}U$ values range from -0.13‰ to -0.75‰ (Table S2). Each sample was analyzed in triplicate with an average 2σ error of 0.07‰ and analysis of

standards yielded an internal precision (2σ) of 0.1‰. The rugose coral fragment is 0.12‰ lower than coeval bulk limestone supporting previous reports by Romaniello et al. (2013) that post-depositional cementation shifts bulk limestone to higher values. Two negative isotopic excursions are observed and labeled D1 and D2 (Fig. 1). The D1 event begins near the *jamieae* – lower *rhenana* zone boundary and ends in the mid-*linguiformis* Zone with a ~0.2‰ negative shift. The D2 excursion starts in the lower *triangularis* Zone and ends in the middle of the upper *triangularis* Zone with a ~0.3‰ negative shift. Using biostratigraphically and radiometrically (Becker et al., 2012) controlled average sedimentation rates (~13-33 m/My) calculated for the Devil's Gate section, the approximate duration of the event D1 is 3.8 My and D2 is 1.1 My.

4.2 Additional geochemical analysis

Selected whole rock and carbonate fraction elemental concentrations are shown in Table S2. No significant correlations among $\delta^{238}U$ and measured elemental concentrations are observed (Fig. 2, Fig. S2). Wt% insoluble residues range from 7% to 28% with an average of 14% and show no co-variance with $\delta^{238}U$ values (Fig. S2). TOC values are low, ranging from 0.13% to 0.77% with an average of 0.26% and a cross plot of $\delta^{238}U$ against TOC shows no correlation (Fig. 2).

$\delta^{13}C$ values range from -1.4‰ to 3.7‰ and $\delta^{18}O$ values between -13.5‰ to -5.3‰ (Fig. 1; Table S2). The measured $\delta^{13}C$ trends are similar to those reported by Joachimski et al. (2002) for the Devil's Gate location with two positive excursions peaking in the upper *rhenana* and lower to middle *triangularis* zones. These two

excursions correspond to other previously reported Late Devonian positive excursions across the globe (Fig. 1; McGhee et al., 1986; Buggisch, 1991; Joachimski and Buggisch, 1993; Joachimski et al., 2002; Stephens and Sumner, 2003). The older $\delta^{13}C$ excursion (late *rhenana* Zone) records a ~2‰ positive shift, overlaps in time with, but is shorter than, the D1 negative $\delta^{238}U$ excursion, and coincides with the late Frasnian extinction (LKW) pulse. The younger $\delta^{13}C$ excursion begins in the *linguiformis* Zone, records a ~+4‰ shift that is coincident with the four main F-F extinction pulses (UKW), and it begins before the onset and peak of the D2 negative $\delta^{238}U$ excursion (Fig. 1). There is no co-variation between $\delta^{13}C$ and $\delta^{238}U$ values (Fig. S2). $\delta^{18}O$ values are uniformly low (average = -7.8‰; Fig. S2, Table S2) and show no systematic stratigraphic trends with $\delta^{13}C$, $\delta^{238}U$, or extinction pulses suggesting that the low values represent overprinting by elevated temperatures during burial diagenesis. The fact that U-isotope shifts are maintained despite clear overprinting of $\delta^{18}O$ values suggests that $\delta^{238}U$ values may be fairly resistant to diagenetic alteration.

5.0 DISCUSSION

5.1 Evaluating depositional and diagenetic influences

We evaluate potential local influences on the measured $\delta^{238}U$ curve using relationships between observed facies and comparisons among elemental, $\delta^{13}C$, TOC, and wt% insoluble residues. The D1 and D2 negative $\delta^{238}U$ excursions do not systematically coincide with Devil's Gate anoxic facies or with recognized transgressive-regressive facies patterns (Fig. 1). For example, moderately anoxic

limestone-marl rhythmite facies forming the transgressive systems tract and maximum flooding zones for all six of the depositional sequences record the lowest as well as the highest $\delta^{238}U$ values (Fig. S3). Likewise, facies deposited during high $\delta^{238}U$ values (indicating more oxic conditions) near the F-F boundary and upper *triangularis* Zone are anoxic to moderately anoxic (Fig. 1). In addition, the D1 and D2 negative intervals cross cut sequence boundaries (D1) or start and end in mid sequence (D2) indicating no relationship with water-depth changes. RSM, TOC, and Mn/Sr ratios were analyzed to assess local redox conditions in bottom waters or pore waters and no co-variance is observed indicating $\delta^{238}U$ values do not reflect local conditions (Figs. 2, S2, S4). These relationships indicate that the $\delta^{238}U$ trends are not influenced by local bottom water or pore water redox conditions or water-depth changes.

To test for influences from local detrital siliciclastic sediment or riverine water input, we compare $\delta^{238}U$ values to Al, U, and Th concentrations in whole rock (for detrital sediment influence) and carbonate fractions (for riverine water influence) and to wt% insoluble residues (Fig. 2, Fig. S2). Of these various proxies, only a weak co-variance with Al and Mo is observed ($p = 0.167$ and $p = 0.105$, respectively). Finally, no evidence for subaerial exposure during shallowing facies trends was observed in the studied deeper water succession and Mg/Ca ratios from all samples are less than 0.1 indicating the deposits have not been dolomitized (Table S2).

The $\delta^{238}U$ enrichment of 0.12‰ of the bulk carbonate compared to the coeval low-Mg calcite rugose coral fragment (Table S2) supports earlier studies of Romaniello et al. (2013) and Chen et al. (*submitted*) who report a 0.1‰ to 0.4‰ enrichment of modern and Neogene carbonates due to the addition of secondary calcite precipitated from low-oxygen pore waters. We argue that this diagenetic overprinting was relatively uniform over the 140 m-thick succession because the samples were all derived from micrite-dominated facies and record consistently low $\delta^{18}O$ values which indicate uniform geothermal gradients and burial depths. The interpretation of the preservation of original secular seawater trends is supported by previous studies reporting similar $\delta^{238}U$ trends among globally separated Upper Permian-Lower Triassic successions all of which experienced diverse diagenetic histories (Brennecka et al., 2011; Lau et al., 2016; Elrick et al., 2017). The measured Late Devonian $\delta^{13}C_{carb}$ trends are similar to those reported from geographically widespread locations (Joachimski and Buggisch, 1993; Joachimski et al., 2002; Godderis and Joachimski, 2004; van Geldern et al., 2006; Song et al., 2017) which also supports the interpretation that the $\delta^{238}U$ curve preserves a global seawater signal. In summary, given the results from comparisons among facies and stratigraphic trends, elemental, TOC, wt% insoluble proxies, and the $\delta^{13}C$ trends, we interpret that the measured $\delta^{238}U$ curve represents a record of global-ocean redox variations.

Recently, Song et al. (2017) report $\delta^{238}U$ trends from carbonates spanning <4.5 My of the Late Devonian from Baisha, South China. Average isotopic values from South China (-0.26‰) are slightly enriched compared to average Devil's Gate

values (-0.39‰) and three negative $\delta^{238}U$ excursions are identified with magnitudes of shift of <-0.3‰ (Fig. S5). Two of the negative excursions, which are defined by only one to three data points, partly overlap in time with the D1 and D2 excursions (upper *rhenana* and middle *triangularis* zones) with the remaining negative excursion reaching its lowest value in the *linguiformis* Zone when the Devil's Gate curve is shifting back to higher isotopic values. The overlap in timing between two of the negative excursions (though apparently briefer in South China) supports interpretations that this portion of the $\delta^{238}U$ curves represent global seawater redox trends. The apparent mismatch in $\delta^{238}U$ trends between the two Late Devonian study sites during the upper *rhenana* through lower *linguiformis* zones may be due to increased tectonic subsidence in the South China pull-apart basin which induced basin deepening, restricted current circulation and oxygen-depletion as well as upwelling of hydrothermal fluids (Chen et al., 2001; 2006), and uncertainties in the precise position of their conodont zonal boundaries. Moreover, a portion of the Late Devonian $\delta^{238}U$ shifts occur within a single conodont zone, therefore the exact timing of the shift within that zone cannot be determined. If the apparent mismatch in $\delta^{238}U$ trends between this study and South China were due to overprinting by local depositional or diagenetic processes, then the original $\delta^{238}U$ values would increase rather than decrease. This is because detrital sediment or riverine waters are enriched in $\delta^{238}U$ as are cements from oxygen-depleted pore waters. Given this, $\delta^{238}U$ curves with lower values more likely represent original seawater redox conditions. Ultimately, additional $\delta^{238}U$ studies of this time interval

from other contemporaneous sections are required to unravel the apparent mismatch.

Song et al. (2017) report a mostly positive relationship between measured $\delta^{238}U$ and $\delta^{13}C$ values and therefore infer that increased ocean anoxia was linked to climatically controlled, lower surface water productivity. In contrast, $\delta^{238}U$ and $\delta^{13}C$ relationships in this study do not show co-varying trends (Fig. S2). For example, the onset and duration of both Devil's Gate positive $\delta^{13}C$ excursions do not coincide with the onset and full duration of D1 and D2 $\delta^{238}U$ events which implies that the processes controlling organic carbon sequestration were temporally, and perhaps spatially, decoupled from those controlling ocean anoxia. Similar temporal decoupling between $\delta^{238}U$ and $\delta^{13}C$ records over a range of geologic time periods is reported by Brennecka et al. (2011), Dahl et al. (2014), Lau et al. (2016), Elrick et al. (2017), and Bartlett et al. (*in review*).

5.2 Extinction versus anoxic sediment and global ocean $\delta^{238}U$ curve

To evaluate relationships between Late Devonian extinction pulses and local seawater anoxia, we compile the occurrence and timing of marine facies defined as anoxic, intermittently anoxic, and oxic/suboxic from available Upper Devonian data with conodont zonation-level age control (Fig. 3; see discussion in Supplementary Information). The compilation is dominated by successions composed of deeper-water facies accumulating below wave base so as to minimize the effects of local shallow-water oxygenation by simple diffusion/wave mixing with atmospheric oxygen. We acknowledge that not all organic-rich mudrocks are indicative of

sustained bottom water anoxia and not all sediments deposited in anoxic bottom waters are 'black shales' (for example, turbidites or organic-rich limestone); however, we agree with Melchin et al. (2013) that this approach provides a sufficient first-order proxy to identify anoxic depositional conditions. It is important to emphasize that except for rare occasions (cf., Dopieralska et al., 2006; Carmichael et al., 2014), available Devonian marine deposits accumulated in epeiric seas or flooded continental margins rather than on oceanic crust in open-ocean settings (which have since been subducted). Given this, our compiled sediment record represents dominantly low-latitude epeiric sea anoxia trends which may or may not track the conditions in open-ocean seawaters. The compiled sediment redox data spans the studied ~7 My time interval and is derived from five different paleocontinents, an island arc, and an accretionary complex located in tropical to subtropical paleolatitudes (Fig. S1). These epeiric seas were, however, presumably where the bulk of Late Devonian benthic organisms lived and biodiversity records from these deposits provide a robust record of Devonian extinction trends.

The late Frasnian extinction pulse (LKW) occurs during a time when nearly half (45%) of the compiled epeiric sea sites accumulated anoxic or intermittently anoxic deposits (Fig. 3; see SI for discussion on calculating epeiric sea areas). The F-F extinction pulses (UKW) overlap in time with anoxic or moderately anoxic deposition in ~70% of the compiled sites including the Asian island arc and Thailand accretionary complex (Fig. 3). These results support previous interpretations that anoxic conditions in epeiric seas and more open-ocean locations were associated with the Late Devonian extinction pulses. This

comparison, however, does not address the relationships between the *global* seawater signal afforded by the $\delta^{238}U$ curve and low-latitude epeiric sea sediment records.

The comparison between the compiled subtropical dominantly epeiric sea sediment redox record and the global-ocean $\delta^{238}U$ curve indicates that the two records generally track each other except during the main F-F extinction interval (Fig. 3). Beginning at the base of the section, just prior to the D1 excursion (upper *hassi-jamieae* zones) when $\delta^{238}U$ trends suggest more oxic global seawaters, >60% of the subtropical locations also accumulated oxic/suboxic deposits indicating that epeiric seas redox conditions were generally coupled with the global oceans. During the D1 anoxic event, 45% of the epeiric sea locations accumulated anoxic deposits and the remaining 55% of locations record oxic/suboxic conditions indicating partial coupling of the two seawater masses. The short time interval between the D1 and D2 excursions during the most intense Late Devonian extinction pulses (UKW), global oceans were more oxic; however, ~70% of the epeiric sea and more open-ocean locations were accumulating anoxic to moderately anoxic deposits indicating the two seawater masses were decoupled. Interestingly, during this same time interval, the South China $\delta^{238}U$ curve also records increasing and higher isotopic values suggesting increasingly oxic seawaters (Fig. S5). During the D2 excursion, ~55% of the sites record anoxic conditions indicating the two seawater masses were partially coupled; whereas after the D2 excursion (latter half of upper *triangularis* Zone), ~65% of the sites record oxic/suboxic conditions indicating general coupling between the two seawater masses. In summary, over the ~7 My

study interval, subtropical epeiric seas were coupled to partially coupled with contemporaneous global oceans except for short interval (<500 ky) straddling the F-F boundary (UKW). This pattern of overall seawater redox coupling provides compelling evidence that shallow epeiric seas were in communication to partial communication with Late Devonian open-ocean seawater and is further supported by numerous studies reporting similar Late Devonian $\delta^{13}C_{carb}$ and $\delta^{18}O_{apatite}$ trends among geographically widespread epeiric sea locations (e.g., Joachimski et al., 2002; Elrick et al., 2009).

The brief interval of time during the UKW event when the $\delta^{238}U$ curve and sediment redox compilation do not match cannot be explained by eustatic sea-level fall and resultant restricted circulation between epeiric seas and the global oceans because both the more open-ocean sites (Thailand and Asian island arc) also record moderately anoxic conditions. Furthermore, the UKW event occurred during the T-R IId-3 eustatic sea-level rise rather than fall, which should have facilitated exchange between the water masses. It might be argued that the eustatic flooding resulted in extensive epeiric seaway development and those relatively shallow subtropical waters were prone to warmer temperatures and lower dissolved oxygen concentrations which resulted in local anoxic conditions separate from the rest of the global oceans. Again, the fact that the more open sites also record moderately anoxic conditions argues against oxygen solubility-temperature controls. Local temperature-controlled seawater oxygen solubility changes are also not supported by Late Devonian $\delta^{18}O$ trends (Fig. S5; Joachimski and Buggisch, 2002). At present it is unclear why both the Devil's Gate and South China sections record increasing and

higher $\delta^{238}U$ values when the majority of subtropical compiled sediment sites accumulated anoxic/moderately anoxic deposits.

5.3 U-cycle modeling

From a range of global paleogeographic reconstruction maps, we estimate that about 15% of the entire Late Devonian ocean was comprised of epeiric seas. If we assume that between one quarter to one half of the epeiric sea area, namely the warm subtropical paleolatitudes, accumulated anoxic deposits and sequestered U, then that area would be about 4% to 7.5% of the total Late Devonian seafloor. For comparison, the modern ocean has <0.2% of seafloor accumulating anoxic deposits (Tissot and Dauphas, 2015). This simple visual estimation suggests that anoxia in epeiric seas alone represents 18 to 37 times more area of anoxic sediment accumulation than the modern ocean and implies that global Devonian ocean $\delta^{238}U$ signatures should have been significantly more depleted than modern oceans. The ~-0.39‰ average Devil's Gate $\delta^{238}U$ values include the effects of cement precipitated from poorly oxygenated pore waters (cf., Romaniello et al., 2013). If we remove these diagenetic effects (using a constant 0.27‰ correction factor; see diagenetic factor discussion in SI) from the measured curve, the 'corrected' Late Devonian curve would average -0.7‰, which is significantly lower than modern seawater values of ~-0.4‰ and supports the hypothesis that Late Devonian seawaters were characteristically more reducing than modern seawaters.

To quantitatively estimate changes in area of anoxic seafloor and the flux of seawater U into anoxic sediments, we use a steady-state mass balance model (see SI

for model details and output). The modeling results suggest that during the peak of the D1 excursion there was a ~5% increase (from Late Devonian background values) in the total seafloor accumulating anoxic sediments, whereas at D2 there was a ~15% increase (from background values) in the total area of anoxic seafloor (Fig. S6). The modeling also estimates that during the D1 peak, 65% of seawater U was sequestered into anoxic sediments, whereas during the D2 peak, 82% of seawater U was sequestered into sediments (Fig. S6). Similar modeling ranges of U sequestered into Paleozoic anoxic sediments is reported by Brennecka et al. (2011), Lau et al. (2016), and Elrick et al. (2017) during the Late Permian mass extinction and by Song et al. (2017) for the Late Devonian extinction. Regardless of the exact percentages of U sequestration during the negative excursions, it is apparent that there was substantial U drawdown during anoxic events which has implications for decreasing U residence times from the modern value of ~400 ky. The results of our model suggest that Late Devonian events D1 and D2 reflect ~40% and ~60% decreases in U residence time, respectively.

6.0 CONCLUSIONS

1) A high-resolution $\delta^{238}U$ curve across ~7 My of the Late Devonian was developed to test the hypothesis that widespread marine anoxia was coincident with Late Devonian extinction pulses (the late Frasnian lower Kellwasser and the Frasnian-Famennian boundary upper Kellwasser events). The measured $\delta^{238}U$ curve shows no co-variation among local anoxic facies, transgressive-regressive facies trends, redox-sensitive metals, TOC, Mg/Ca and Mn/Sr ratios, or detrital elements and

insoluble residue proxies indicating that $\delta^{238}U$ variabilities were not controlled by local depositional or diagenetic processes and represent global-ocean redox conditions.

2) Two negative excursions, termed D1 (late Frasnian) and D2 (early Famennian), indicating more reducing global seawater conditions are recorded with magnitudes of -0.2‰ to -0.3‰, respectively. The onset and demise of both excursions are gradual with the D1 spanning ~3.8 My and D2 spanning ~1.1 My. Steady-state mass balance modeling of the $\delta^{238}U$ trends suggest that there was a ~5% to 15% increase (from background Late Devonian values) in total ocean seafloor area accumulating anoxic deposits and a ~65% to 82% increase in the flux of seawater U to anoxic deposits during the D1 and D2 anoxic events, respectively.

3) The redox characteristics of well-dated Upper Devonian marine deposits from subtropical deeper water epeiric sea and more open-ocean sites were compiled to compare with the measured $\delta^{238}U$ curve and the main Late Devonian extinction pulses. The overlap in timing between subtropical epeiric sea and open-ocean anoxic sediment accumulation and the main extinction pulses support earlier interpretations that anoxia played an important role in the Late Devonian biodiversity crisis. Comparisons between the timing of anoxic epeiric sea and open-ocean deposits and the global seawater $\delta^{238}U$ redox curve indicates overall coupling between the two seawater masses for much of the studied time interval, except for a brief interval (<500 ky) of decoupling during the main F-F extinction event (UKW).

7.0 REFERENCES

Algeo, T.J., and Scheckler, S.E., 1998, Terrestrial-marine teleconnections in the Devonian: links between the evolution of land plants, weathering processes, and marine anoxic events: Philosophical Transactions of the Royal Society of London B, v. 353, p. 113-130, doi: 10.1098/rstb.1998.0195.

Algeo, T.J., Berner, R.A., Maynard, J.B., and Scheckler, S.E., 1995, Late Devonian ocean anoxic events and biotic crises: "rooted" in the evolution of vascular land plants?: GSA Today, v. 5, p. 64-66.

Bambach, R.K., Knoll, A.H., and Wang, S.C., 2004, Origination, extinction, and mass depletions of marine diversity: Paleobiology, v. 30, p. 522-542, doi: 10.1666/0094-8373(2004)030<0522:OEAMIDO>2.0.CO;2.

Bartlett, R., Elrick, M., Wheeley, J.R., Polyak, V., Desrochers, A., and Asmerom, Y., *in review*, Abrupt global-ocean anoxia during the Late Ordovician-early Silurian detected using uranium isotopes of marine carbonates.

Becker, R.T., Gradstein, F.M., and Hammer, O., 2012, The Devonian Period, *in* Gradstein, F.M., et al., eds., The Geologic Time Scale 2012: Amsterdam, Elsevier, v. 2, p. 559-601, doi: 10.1016/B978-0-444-59425-9.00022-6.

Bigeleisen, J., 1996, Temperature dependence of the isotope chemistry of the heavy elements: Proceedings of the National Academy of Sciences, v. 93, p. 9393-9396.

Blakey, R.C., 2016, Colorado Plateau Geosystems [WWW Document], URL: http://deeptimemaps.com/wp-content/uploads/2016/05/380_Ma_Dev_GPT-1.png; http://deeptimemaps.com/wp-content/uploads/2016/05/NAM_key-375Ma_LDev.png

Bond, D.P.G., and Grasby, S.E., 2016, On the causes of mass extinctions: Palaeogeography, Palaeoclimatology, Palaeoecology, v. 478, p. 3-29, doi: 10.1016/j.palaeo.2016.11.005.

Bond, D.P.G., and Wignall, P.B., 2008, The role of sea-level change and marine anoxia in the Frasnian-Famennian (Late Devonian) mass extinction: Palaeogeography, Palaeoclimatology, Palaeoecology, v. 263, p. 107-118, doi: 10.1016/j.palaeo.2008.02.015.

Bond, D., Wignall, P.B., and Racki, G., 2004, Extent and duration of marine anoxia during the Frasnian-Famennian (Late Devonian) mass extinction in Poland, Germany, Austria and France: Geological Magazine, v. 141, p. 173-193, doi: 10.1017/S0016756804008866.

Bratton, J.F., Berry, W.B.N., and Morrow, J.R., 1999, Anoxia pre-dates Frasnian-Famennian boundary mass extinction horizon in the Great Basin, USA: Palaeogeography, Palaeoclimatology, Palaeoecology, v. 154, p. 275-292, doi: 10.1016/S0031-0182(99)00116-9.

Brennecka, G.A., Herrmann, A.D., Algeo, T.J., and Anbar, A.D., 2011, Rapid expansion of oceanic anoxia immediately before the end-Permian mass extinction: National Academy of Sciences Proceedings, v. 108, p. 17,631-17634, doi: 10.1073/pnas.1106039108.

Buggisch, W., 1991, The global Frasnian-Famennian 'Kellwasser Event': Geologische Rundschau, v. 80, p. 49-72, doi: 10.1007/BF01828767.

Caputo, M.V., 1985, Late Devonian glaciation in South America: Palaeogeography, Palaeoclimatology, Palaeoecology, v. 51, p. 291-317, doi: 10.1016/0031-0182(85)90090-2.

Caputo, M.V., Melo, J.H.G., Streel, M., and Isbell, J.L., 2008, Late Devonian and Early Carboniferous glacial records of South America: The Geological Society of America, Special Paper 441, p. 1-13, doi: 10.1130/2008.244(11).

Carmichael, S.K., Waters, J.A., Suttner, T.J., Kido, E., and Dereuil, A.A., 2014, A new model for the Kellwasser Anoxia Events (Late Devonian): Shallow water anoxia in an open oceanic setting in the Central Asian Orogenic Belt: Palaeogeography, Palaeoclimatology, Palaeoecology, v. 399, p. 394-403, doi: 10.1016/j.palaeo.2014.02.016.

Chen, D., Tucker, M.E., Zhu, J., and Jian, M., 2001, Carbonate sedimentation in a starved pull-apart basin, Middle to Late Devonian, southern Guilin, South China, Basin Research, Basin Research, v. 13, p. 141-167.

Chen, D., Qing, H., Xin, Y., and Li, H., 2006, Hydrothermal venting and basin evolution (Devonian South China): constraints from rare earth element geochemistry of chert, Sedimentary Geology v. 183, p. 203–216, doi: 10.1016/j.sedgeo.2005.09.020.

Chen, X., Romaniello, S.J., Herrmann, A.D., Hardisty, D., Swart, P.K., Gill, B.C., and Anbar, A.D., 2017, *submitted*, Diagenetic effects on uranium isotope fractionation in carbonate sediments from the Bahamas.

Cheng, H., Edwards, R.L., Shen, C.C., Polyak, V.J., 2013, Improvements in ^{230}Th dating, ^{230}Th and ^{234}U half-life values, and U-Th isotopic measurements by multi-collector inductively coupled plasma mass spectrometry: Earth and Planetary Science Letters, v. 371-372, p. 82-91, doi: 10.1016/j.epsl.2013.04.006.

Copper, P., 1986, Frasnian/Famennian mass extinction and cold-water oceans: Geology, v. 14, p. 835-839, doi: 10.1130/0091-7613(1986)14<835:FMEACO>2.0.CO;2.

Copper, P., 2002, Reef development at the Frasnian/Famennian mass extinction boundary: Palaeogeography, Palaeoclimatology, Palaeoecology, v. 181, p. 27-65, doi: 10.1016/S0031-0182(01)00472-2.

Dahl, T.W., Boyle, R.A., Canfield, D.E., Connelly, J.N., Gill, B.C., Lenton, T.M., and Bizzarro, M., 2014, Uranium isotopes distinguish two geochemically distinct stages during the late Cambrian SPICE event: Earth and Planetary Science Letters, v. 401, p. 313-326, doi: 10.1016/j.epsl.2014.05.043.

Day, J., and Witzke, B.J., 2017, Upper Devonian biostratigraphy, event stratigraphy, and Late Frasnian Kellwasser extinction bioevents in the Iowa Basin: Western Euramerica: Stratigraphy and Timescales, v. 2, p. 243-332, doi: 10.1016/bs.sats.2017.08.002.

Dopieralska, J., Belka, Z., and Haack, U., 2006, Geochemical decoupling of water masses in the Variscan oceanic system during Late Devonian times: Palaeogeography, Palaeoclimatology, Palaeoecology, v. 240, p. 108-119, doi: 10.1016/j.palaeo.2006.03.056.

Elrick, M., and Witzke, B., 2016, Orbital-scale glacio-eustasy in the Middle Devonian detected using oxygen isotopes of conodont apatite: Implications for long term greenhouse-icehouse climatic transitions: Palaeogeography, Palaeoclimatology, Palaeoecology, v. 445, p. 50-59, doi: 10.1016/j.palaeo.2015.12.019.

Elrick, M., Berkyova, S., Klapper, G., Sharp, Z., Joachimski, M., and Fryda, J., 2009, Stratigraphic and oxygen isotope evidence for My-scale glaciation driving eustasy in the Early-Middle Devonian greenhouse world: Palaeogeography, Palaeoclimatology, Palaeoecology, v. 276, p. 170-181, doi: 10.1016/j.palaeo.2009.03.008.

Elrick, M., and Witzke, B., 2016, Orbital-scale glacio-eustasy in the Middle Devonian detected using oxygen isotopes of conodont apatite: Implications for long term greenhouse-icehouse climatic transitions: Palaeogeography, Palaeoclimatology, Palaeoecology, v. 445, p. 50-59, doi: 10.1016/j.palaeo.2015.12.019.

Elrick, M., Polyak, V., Algeo, T.J., Romaniello, S., Asmerom, Y., Herrmann, A.D., Anbar, A.D., Zhao, L., Chen, Z., 2017, Global-ocean redox variation during the middle-late Permian through Early Triassic based on uranium isotope and Th/U trends of marine carbonates: Geology, v. 45, p. 163-166, doi: 10.1130/G38585.1.

Feist, R., 1985, Devonian stratigraphy of the Southeastern Montagne Noire (France): Cour. Forsch.-Inst. Senckenberg, v. 75, p. 331-352.

Formolo, M.J., Riedinger, N., and Gill, B.C., 2014, Geochemical evidence for euxinia during the Late Devonian extinction events in the Michigan Basin (U.S.A.): Palaeogeography, Palaeoclimatology, Palaeoecology, v. 414, p. 146-154, doi: 10.1016/j.palaeo.2014.08.024.

Frakes, L.A., Francis, J.E., and Syktus, J.I., 2005, Climate modes of the Phanerozoic: Cambridge University Press.

George, A.D., Chow, N., Trinajstic, and K.M., 2014, Oxic facies and the Late Devonian mass extinction, Canning Basin, Australia: Geology, v. 42, p. 327-330, doi: 10.1130/G35249.1.

Giles, K.A., and Dickinson, W.R., 1995, The interplay of eustasy and lithospheric flexure in forming stratigraphic sequences in foreland settings: an example from the Antler foreland, Nevada and Utah: Stratigraphic evolution of foreland basins, SEPM Special Publication No. 52, doi: 10.2110/pec.95.52.0187.

Godderis, Y., and Joachimski, M.M., 2004, Global change in the Late Devonian: modelling the Frasnian-Famennian short-term carbon isotope excursions: Palaeogeography, Palaeoclimatology, Palaeoecology, v. 202, p. 309-329, doi: 10.1016/S0031-0182(03)00641-2.

Goodfellow, W.D., Geldsetzer, H., McLaren, D.J., Orchard, M.J., and Klapper, G., 1989, Geochemical and isotopic anomalies associated with the Frasnian-Famennian extinction: Historical Biology, v. 2, p. 51-72, doi: 10.1080/08912968909386490.

Gutschick, R.C., and Sandberg, C.A., 1991, Late Devonian history of Michigan Basin *in* Catacosinos, P.A., and Daniels, P.A., eds., Early sedimentary evolution of the Michigan Basin: Geological Society of America Special Paper 256, p. 181-202, doi: 10.1130/SPE256-p181.

Hallam, A., and Wignall, P.B., 1997, Mass extinctions and their aftermath: Oxford University Press, UK.

Hood, A.S., Planavsky, N.J., Wallace, M.W., Wang, X., Bellefroid, E.J., Gueguen, B., and Cole, D.B., 2016, Integrated geochemical-petrographic insights from component-selective $\delta^{238}U$ of Cryogenian marine carbonates: Geology, v. 44, p. 935-938, doi: 10.1130/G38533.1.

Isaacson, P.E., Diaz-Martinez, E., Grader, G.W., Kalvoda, J., Babek, O., and Devuyst, F.X., 2008, Late Devonian-earliest Mississippian glaciation in Gondwanaland and its biogeographic consequences: Palaeogeography, Palaeoclimatology, Palaeoecology, v. 268, p. 126-142, doi: 10.1016/j.palaeo.2008.03.047.

Ji, Q., 1994, On the Frasnian-Famennian extinction event in South China as viewed in the light of conodont study, Prof. Pap. Stratigr. Palaeontol., v. 24, p. 79-109 (in Chinese with English abstract).

Joachimski, M.M., and Buggisch, W., 1993, Anoxic events in the late Frasnian-Causes of the Frasnian-Famennian faunal crisis?: Geology, v. 21, p. 675-678, doi: 10.1130/0091-7613(1993)021<0675:AEITLF>2.3.CO;2.

Joachimski, M.M., and Buggisch, W., 2002, Conodont apatite $\delta^{18}O$ signatures indicate climatic cooling as a trigger of the Late Devonian mass extinction: Geology, v. 30, p. 711-714, doi: 10.1130/0091-7613(2002)030<0711:CAOSIC>2.0.CO;2.

Joachimski, M.M., Pancost, R.D., Freeman, K.H., Ostertag-Henning, C., and Buggisch, W., 2002, Carbon isotope geochemistry of the Frasnian-Famennian transition: Palaeogeography, Palaeoclimatology, Palaeoecology, v. 181, p. 91-109, doi: 10.1016/S0031-0182(01)00474-6.

Johnson, J.G., Klapper, G., and Sandberg, C.A., 1985, Devonian eustatic fluctuations in Euramerica: Geological Society of America Bulletin, v. 96, p. 567-587, doi: 10.1130/0016-7606(1985)96<567:DEFIE>2.0.CO;2.

Kaiho. K., Yatsu, S., Masahiro, O. Gorjan, P., Casier, J-G., Masayuki, I., 2013, A forest fire and soil erosion event during the Late Devonian mass extinction, Palaeogeography, Palaeoclimatology, Palaeoecology, v. 392, p. 272–280.

Kiessling, W., and Simpson, C., 2011, On the potential for ocean acidification to be a general cause of ancient reef crises: Global Change Biology, v. 17, p. 56-67, doi: 10.1111/j.1365-2486.2010.02204.x.

Kiessling, W., Flugel, E., and Golonka, J., 2000, Fluctuations in the carbonate production of Phanerozoic reefs, *in* Insalaco, E., Skelton, P.W., and Palmer, T.J., eds., Carbonate Platform Systems: components and interactions: Geological Society London Special Publications, v. 178, p. 191-215, doi: 10.1144/GSL.SP.2000.178.01.13.

Klinkhammer, G.P., and Palmer, M.R., 1991, Uranium in the oceans: Where it goes and why?: Geochimica et Cosmochimica Acta, v. 55, p. 1799-1806, doi: 10.1016/0016-7037(91)90024-Y.

Konigshof, P., Savage, N.M., Lutat, P., Sardsud, A., Dopieralska, J., Belka, Z., and Racki, G., 2012, Late Devonian sedimentary record of the Paleotethys Ocean – the Mai Sariang section, northwestern Thailand: Journal of Asian Earth Sciences, v. 52, p. 146–157, doi: 10.1016/j.jseaes.2012.03.006.

Ku, T., Knauss, K.G., and Mathieu, G.G., 1977, Uranium in open ocean: concentration and isotopic composition: Deep-Sea Research, v. 24, p. 1005-1017, doi: 10.1016/0146-6291(77)90571-9.

Lau, K.V., Maher, K., Altiner, D., Kelley, B.M., Kump, L.R., Lehrmann, D.J., Silva-Tamayo, J.C., Weaver, K.L., Yu, M., and Payne, J.L., 2016, Marine anoxia and delayed Earth system recovery after the end-Permian extinction: National Academy of Sciences Proceedings, v. 113, p. 2360-2365, doi: 10.1073/pnas.1515080113.

Lau, K.V., Macdonald, F.A., Maher, K., and Payne, J.L., 2017, Uranium isotope evidence for temporary ocean oxygenation in the aftermath of the Sturtian Snowball Earth: Earth and Planetary Science Letters, v. 458, p. 282-292, doi: 10.1016/j.epsl.2016.10.043.

Ma, X.P., and Bai, S.L., 2002, Biological, depositional, microspherule, and geochemical records of the Frasnian/Famennian boundary beds, South China: Palaeogeography, Palaeoclimatology, Palaeoecology, v. 181, p. 325-346, doi: 10.1016/S0031-0182(01)00484-9.

Ma, X., Gong, Y., Chen, D., Racki, G., Chen, X., and Liao, W., 2016, The Late Devonian Frasnian-Famennian Event in South China – Patterns and causes of extinctions, sea level changes, and isotope variations: Palaeogeography, Palaeoclimatology, Palaeoecology, v. 448, p. 224-244, doi: 10.1016/j.palaeo.2015.10.047.

McGhee, G.R., Orth, L.J., Quintana, L.R., Gilmore, J.S., and Olsen, E.J., 1986, Late Devonian 'Kellwasser Event' mass-extinction horizon in Germany: no chemical evidence for a large body impact: Geology, v. 14, p. 776-779, doi: 10.1130/0091-7613(1986)14<776:LDKEMH>2.0.CC.

McGhee, G.R., 1996, The late Devonian mass extinction: the Frasnian/Famennian crisis: Columbia University Press, 303 pg.

McGhee, G.R., 2001, Late Devonian extinction: Palaeobiology II, p. 223-226.

Melchin, M.J., Mitchell, C.E., Holmden, C., and Storch, P., 2013, Environmental changes in the Late Ordovician-early Silurian: Review and new insights from black shales and nitrogen isotopes: GSA Bulletin, v. 125, p. 1635-1670, doi: 10.1130/B30812.1.

Montoya-Pino, C., Weyer, S., Anbar, A.D., Pross, J., Oschmann, W., van de Schootbrugge, B., and Arz, H.W., 2010, Global enhancement of ocean anoxia during Oceanic Anoxic Event 2: A quantitative approach using U isotopes: Geology, v. 38, p. 315-318, doi: 10.1130/G30652.1.

Morford, J.L., and Emerson, S., 1999, The geochemistry of redox sensitive trace metals in sediments: Geochimica et Cosmochimica Acta, v. 63, p. 1735-1750, doi: 10.1016/S0016-7037(99)00126-X.

Morrow, J.R., and Sandberg, C.A., 2008, Evolution of Devonian carbonate-shelf margin, Nevada: Geosphere, v. 4, p. 445-458, doi: 10.1130/GES00134.1.

Over, J.D., 2002, The Frasnian-Famennian boundary in central and eastern United States: Palaeogeography, Palaeoclimatology, Palaeoecology, v. 181, p. 153-169, doi: 10.1016/S0031-0182(01)00477-1.

Over, J.D., 2007, Conodont biostratigraphy of the Chattanooga Shale, Middle and Upper Devonian, Southern Appalachian Basin, Eastern United States: Journal of Paleontology, v. 81, p. 1194-1217, doi: 10.1666/06-056R.1.

Racki, G., 2005, Toward understanding Late Devonian global events: few answers, many questions: Developments in Palaeontology and Stratigraphy, v. 20, p. 5-36, doi: 10.1016/S0920-5446(05)80002-0.

Romaniello, S.J., Herrmann, A.D., and Anbar, A.D., 2013, Uranium concentrations and $^{238}U/^{235}U$ isotope ratios in modern carbonates from the Bahamas: Assessing a novel paleoredox proxy: Chemical Geology, v. 362, p. 305-316, doi: 10.1016/j.chemgeo.2013.10.002.

Sandberg, C.A., and Poole, F.G., 1977, Conodont biostratigraphy and depositional complexes of Upper Devonian cratonic-platform and continental-shelf rocks in the western United States, *in* Murphy, M.A., Berry, W.B., and Sandberg, C.A., eds, Western North America; Devonian – California University, Riverside, Campus Museum Contributions 4, p. 144-182, Riverside, CA.

Sandberg, C.A., Ziegler, W., Dreesen, R., and Butler, J.L., 1988, Part 3: Late Frasnian mass extinction: conodont event stratigraphy, global changes, and possible causes: Courier Forschung-Institut Senckenberg, v. 102, p. 263-307.

Sandberg, C.A., Morrow, J.R., and Warme, J.E., 1997, Late Devonian Alamo Impact Event, Global Kellwasser Events, and Major Eustatic Events, Eastern Great Basin, Nevada and Utah: Brigham Young University Geology Studies, v. 42, p. 129-160.

Sandberg, C.A., Morrow, J.R., Poole, F.G., and Ziegler, W., 2003, Middle Devonian to Early Carboniferous event stratigraphy of Devils Gate and Northern Antelope Range sections, Nevada, U.S.A.: Courier Forschung-Institut Senckenberg, v. 242, p. 187-207.

Sepkoski, J.J., 1996, Patterns of Phanerozoic extinction: a perspective from global data bases, *in* Walliser, O.H., eds., Global Events and Event Stratigraphy in the Phanerozoic: Springer-Verlag, Berlin, p. 35-51, doi: 10.1007/978-3-642-79634-0_4.

Song, H., Song, H., Algeo, T.J., Tong, J., Romaniello, S.J., Zhu, Y., Chu, D., Gong, Y., and Anbar, A.D., 2017, Uranium and carbon isotopes document global-ocean redox-productivity relationships linked to cooling during the Frasnian-Famennian mass extinction: Geology, doi: 10.1130/G39393.1.

Spotl, C., and Vennemann, T.W., 2003, Continuous-flow isotope ratio mass spectrometric analysis of carbonates minerals: Rapid communications in mass spectrometry, v. 17, p. 1004-1006, doi: 10.1002/rcm.1010.

Stephens, N.P., and Sumner, D.Y., 2003, Late Devonian carbon isotope stratigraphy and sea level fluctuations, Canning Basin, Western Australia, Palaeogeography, Palaeoclimatology, Palaeoecology, v. 191, p. 203-219, doi: 10.1016/S0031-0182(02)007141-9.

Stigall, A.L., 2010, Speciation collapse and invasive species dynamics during the Late Devonian “Mass Extinction”: GSA Today, v. 22, p. 4-9, doi: 10.1130/G128A.1.

Stylo, M., Neubert, N., Wang, Y., Monga, N., Romaniello, S.J., Weyer, S., and Bernier-Latmani, R., 2015, Uranium isotopes fingerprint biotic reduction: National Academy of Sciences Proceedings, v. 112, p. 5619-5624, doi: 10.1073/pnas.1421841112.

Tissot, F.L.H., and Dauphas, N., 2015, Uranium isotopic compositions of the crust and ocean: Age corrections, U budget and global extent of modern anoxia: Geochimica et Cosmochimica Acta, v. 167, p. 113-143, doi: 10.1016/j.gca.2015.06.034.

van Geldern, R., Joachimski, M.M., Day, J., Jansen, U., Alvarez, F., Yolkin, E.A., and Ma, X.P., 2006, Carbon, oxygen and strontium isotope records of Devonian brachiopod shell calcite: Palaeogeography, Palaeoclimatology, Palaeoecology, v. 240, p. 47-67, doi: 10.1016/j.palaeo.2006.03.045.

Verbruggen, A., Alonso-Munoz, A., Eykens, R., Kehoe, F., Kuhen, H., Richter, S., and Arbegbe, Y., 2008, Preparation and certification of IRMM-3636, IRMM-3636a and IRMM-3636b: OPOCE, doi: 10.2787/60083.

Wendt, J., and Belka, Z., 1991, Age and depositional environment of Upper Devonian (early Frasnian to early Famennian) black shales and limestones (Kellwasser facies) in the eastern Anti-Atlas, Morocco: Facies, v. 21, p. 51-89, doi: 10.1007/BF02536755.

Weyer, S., Anbar, A.D., Gerdes, A., Gordon, G.W., Algeo, T.J., and Boyle, E.A., 2008, Natural fractionation of $\delta^{238}U$: Geochimica et Cosmochimica Acta, v. 72, p. 345-359, doi: 10.1016/j.gca.2007.11.012.

Whalen, M., De Vleeschouwer, D., Payne, J., Day, J., Over, J., and Claeys, P., 2017, Pattern and timing of the Late Devonian biotic crisis in Western Canada: Insights from carbon isotopes and astronomical calibration of magnetic susceptibility data: *in* Devonian Carbonates: Outcrop analogs, reservoirs, and chronostratigraphy (SEPM Special Publication ed., v. 107, p. 185-201. SEPM Society for Sedimentary Geology.

8.0 SUPPLEMENTARY INFORMATION

8.1 Redox interpretations of compiled Upper Devonian marine deposits

Our sediment compilations documenting the occurrence of Upper Devonian anoxic, moderately or intermittently anoxic, or oxic to suboxic deposits are derived from published stratigraphic columns or written descriptions (references cited in Figure 3 caption). The following sediment types were grouped into the three redox categories.

Anoxic deposits: black shales; calcareous, siliceous, or dolomitic dark shale; laminated siliceous shale, laminated dark chert; dark gray mudrocks lacking benthic skeletal fauna; bituminous dark limestone, lithologies containing pyrite framboid sizes and distributions interpreted by respective authors as anoxic/euxinic bottom waters.

Intermittently or moderately anoxic deposits: rhythmically interbedded limestone and shale/marl (rhythmites) with even to nodular bedding and laminated limestone layers, intervals with alternating anoxic and oxic/suboxic characteristics (e.g., bioturbated lime mudstones interbedded with laminated dark mudrocks lacking benthic skeletal fauna), lithologies containing pyrite framboid sizes and distributions interpreted by respective authors as 'dysoxic' bottom waters, micrite-dominated limestones with low-diversity benthic fauna and lacking bioturbation.

Oxic to suboxic deposits: light gray mudrocks, nodular to strongly bioturbated units, deposits containing benthic skeletal fauna and well bioturbated.

8.2 Modeling seawater U cycling

To quantitatively evaluate the effects of Late Devonian redox changes, we use a steady state mass balance model based in part on previous models of Arnold et al. (2004) and Montoya-Pino et al. (2010) to estimate the fraction of U removed to anoxic facies ($f_{Anox\ flux}$) and the area of anoxic seafloor ($f_{Anox\ area}$) based on the measured $\delta^{238}U$ values. Seawater $\delta^{238}U$ is controlled by the isotopic compositions and relative sizes of the two main sinks (oxic/suboxic sediments and anoxic/euxinic sediments):

$$\delta_{River} = (f_{Anox\ flux})(\delta^{238}U_{Anox}) + \left(1 - f_{Anox\ flux}\right)(\delta^{238}U_{Oxic}) \quad (1)$$

Using the isotopic fractionation (Δ) between seawater and U sinks, this equation can be expressed in terms of $\delta^{238}U_{seawater}$ using the following substitutions for anoxic and oxic sink $\delta^{238}U$ values:

$$\delta^{238}U_{Oxic} = \delta^{238}U_{Seawater} + \Delta_{Oxic} \quad (2)$$

$$U_{Anox} = \delta^{238}U_{Seawater} + \Delta_{Anox} \quad (3)$$

Rearranging this equation, the fraction of U removed to anoxic sediments can be determined:

$$f_{Anox\ flux} = \frac{\delta^{238}U_{River} - \delta^{238}U_{Seawater} - \Delta_{Oxic}}{\Delta_{Anox} - \Delta_{Oxic}} \quad (4)$$

Once the fraction of U removed to anoxic sediments is calculated, we can then use these values in conjunction with rate constants that express estimated metal (U) burial rates (k_{Oxic} and k_{Anox}) to model the area of anoxic seafloor based on seawater

$\delta^{238}U$. Sink U burial rates (J_{oxic} and J_{anox}) can be expressed in moles/year by the equations:

$$J_{Oxic} = k_{Oxic} A_{Oxic} (N_U / V_{Ocean}) \quad (5)$$

$$J_{Anox} = k_{Anox} A_{Anox} (N_U / V_{Ocean}) \quad (6)$$

where N_U is the number of moles of U in the ocean, A_{Oxic} and A_{Anox} represent the area of oxic and anoxic U sinks, respectively, and V_{Ocean} is the volume of the ocean. Because our model recognizes only two U sinks (oxic and anoxic) we know the sum of oxic and anoxic seafloor must equal the total seafloor area and we can define the area of U sink fractions as:

$$f_{Oxic\ area} = \frac{A_{Oxic}}{A_{Ocean}} = 1 - f_{Anox\ area} \quad (7)$$

$$f_{Anox\ area} = \frac{A_{Anox}}{A_{Ocean}} \quad (8)$$

The same relationship can be used to express previously calculated anoxic U sink fractions ($f_{Anox\ flux}$) in terms of sink metal burial rates:

$$f_{Anox\ flux} = \frac{J_{Anox}}{J_{Anox} + J_{Oxic}} \quad (9)$$

Lastly, substituting equations 5 and 6 and rearranging this expression we can solve for the fraction of anoxic seafloor area:

$$f_{Anox\ area} = \frac{f_{Anox\ flux}\, k_{Oxic}}{k_{Anox} + f_{Anox\ flux}(k_{Oxic} - k_{Anox})} \quad (10)$$

Our steady-state model requires assumptions be made to simplify calculating the fraction of U removal to anoxic sediments and the area of anoxic seafloor. These assumptions include: 1) constant U isotopic composition for the riverine source, 2) constant fractionation factors for oxic/suboxic and anoxic/euxinic sinks, 3) constant U burial rates, and 4) constant diagenetic correction factor to account for ^{238}U enrichment during the formation of secondary carbonate phases in poorly oxygenated pore waters.

Recent studies characterizing the marine uranium cycle can be used to help identify the range and appropriate parameter values for steady state modeling of U. Andersen et al. (2016) report modern δ^{238}_{River} as -0.27(±0.16)‰, with a range of -0.72‰ to 0.06‰. For our calculations, we utilize an average continental crust $\delta^{238}U$ value of -0.29‰ (Tissot and Dauphas, 2015) as this estimate displays significantly less isotopic variability than reported riverine values. Reported estimates of Δ_{Anox} range from 0.5‰ (Weyer et al., 2008) to 0.77‰ (Stirling et al., 2015). We utilize a value of 0.77‰ in our model calculations based on the most recent data from Kyllaren Fjord, Norway (Noordmann et al., 2015) and laboratory experiments (Stirling et al., 2015) estimating Δ_{Anox} values in this range. Model parameters were set to 0‰ for Δ_{Oxic} based on recent laboratory experiments by Chen et al. (2016) that show primary marine calcite incorporates U from oxic waters with no observed fractionation. We utilize U burial rates (k_{Anox} and k_{Oxic}) of 629 m/year and 29 m/year for anoxic and oxic settings, respectively, based on median values of compiled data from Zheng et al. (2002), Dunk et al. (2002), and McManus et al. (2006). Romaniello et al. (2013) first reported that shallow-buried (<40 cm)

modern carbonate sediments were isotopically enriched by 0.2‰ and 0.4‰. This range of diagenetic effects has been refined using Neogene drill core data from the Bahamas Drilling Project (Unda, Clino, and site 1006) which suggest an average diagenetic correction factor for these fully lithified platform top and basin deposits of 0.27‰ +/- 0.14‰ (Chen et al., *submitted*). For our model calculations, we assume this diagenetic correction factor of +0.27‰. Larger enrichment effects are less likely once the buried and partially cemented sediments move out of communication with bottom waters and U diffusion.

To characterize the effects parameter uncertainty has on model output, we ran sensitivity tests in which model parameters were varied independently across a range of reported values; those sensitivity runs with output U removal fluxes of >100% were deemed unreasonable. Varying $\delta^{238}U_{River}$ between -0.29‰ to -0.5‰ yields anoxic seafloor area estimates ranging from 3% to 8% for event D1 and 5% to 17% for D2. Δ_{Anox} values between 0.63‰ and 0.77‰ return estimates of 8% to 15% anoxic seafloor areas for event D1 and 17% to 99% anoxic seafloor areas for event D2, respectively. Variation of oxic metal burial rates (k_{Oxic}) between 20 m/year and 60 m/year results in estimates of 6% to 15% anoxic seafloor area for event D1, and 12% to 31% for event D2. Anoxic U burial rates between 300 m/year and 900 nmol m/year for k_{Anox} produce ranges of 5% to 15% anoxic seafloor area for the D1 event, and 12% to 30% for the D2 event. Lastly, varying the diagenetic correction factor from 0.25‰ to 0.4‰ results in a range of 7% to 17% for event D1 and between 14% and 77% for event D2.

9.0 SI REFERENCES

Andersen, M.B., Vance, D., Morford, J.L., Bura-Nakic, E., Breitenbach, S.F.M., and Och, L., 2016, Closing in on the marine $^{238}U/^{235}U$ budget: Chemical Geology, v. 420, p. 11-22, doi: 10.1016/j.chemgeo.2015.10.041.

Arnold, G.L., Anbar, A.D., Barling, J., and Lyons, T.W., 2004, Molybdenum isotope evidence for widespread anoxia in Mid-Proterozoic oceans: Science, v. 304, p. 87-90, doi: 10.1126/science.1091785.

Chen, X., Romaniello, S.J., Herrmann, A.D., Wasylenki, L.E., and Anbar, A.D., 2016, Uranium isotope fractionation during coprecipitation with aragonite and calcite: Geochimica et Cosmochimica Acta, v. 188, p. 189-207, doi: 10.1016/j.gca.2016.05.022.

Chen, X., Romaniello, S.J., Herrmann, A.D., Hardisty, D., Swart, P.K., Gill, B.C., and Anbar, A.D., 2017, *in prep*, Diagenetic effects on uranium isotope fractionation in carbonate sediments from the Bahamas.

Dunk, R.M., Mills, R.A., and Jenkins, W.J., 2002, A reevaluation of the oceanic uranium budget for the Holocene: Chemical Geology, v. 190, p. 45-67, doi: 10.1016/S0009-2541(02)00110-9.

McManus, J., Berelson, W.M., Severmann, S., Poulson, R.L., Hammon, D.E., Klinkhammer, G.P., and Holm, C., 2006, Molybdenum and uranium geochemistry in continental margin sediments: Paleoredox potential: Geochimica et Cosmochimica Acta, v. 70, p. 4643-4662, doi: 10.1016/j.gca.2006.06.1564.

Montoya-Pino, C., Weyer, S., Anbar, A.D., Pross, J., Oschmann, W., van de Schootbrugge, B., and Arz, H.W., 2010, Global enhancement of ocean anoxia during Oceanic Anoxic Event 2: A quantitative approach using U isotopes: Geology, v. 38, p. 315-318, doi: 10.1130/G30652.1.

Noordmann, J., Weyer, S., Montoya-Pino, C., Dellwig, O., Neubert, N., Eckert, S., Paetzel, M., and Bottcher, M.E., 2015, Uranium and molybdenum isotope systematics in modern euxinic basins: Case studies from the central Baltic Sea and Kyllaren fjord (Norway): Chemical Geology, v. 396, p. 182-195, doi: 10.1016/j.chemgeo.2014.12.012.

Romaniello, S.J., Herrmann, A.D., and Anbar, A.D., 2013, Uranium concentrations and $^{238}U/^{235}U$ isotope ratios in modern carbonates from the Bahamas: Assessing a novel paleoredox proxy: Chemical Geology, v. 362, p. 305-316, doi: 10.1016/j.chemgeo.2013.10.002.

Stirling, C.H., Andersen, M.B., Warthmann, R., and Halliday, A.N., 2015, Isotope fractionation of ^{238}U and ^{235}U during biologically-mediated uranium reduction: Geochimica et Cosmochimica Acta, v. 163, p. 200-218, doi: 10.1016/j.gca.2015.03.017.

Tissot, F.L.H., and Dauphas, N., 2015, Uranium isotopic compositions of the crust and ocean: Age corrections, U budget and global extent of modern anoxia: Geochimica et Cosmochimica Acta, v. 167, p. 113-143, doi: 10.1016/j.gca.2015.06.034.

Weyer, S., Anbar, A.D., Gerdes, A., Gordon, G.W., Algeo, T.J., and Boyle, E.A., 2008, Natural fractionation of $\delta^{238}U$: Geochimica et Cosmochimica Acta, v. 72, p. 345-359, doi: 10.1016/j.gca.2007.11.012.

Zheng, Y., Anderson, R.F., van Geen, A., and Fleisher, M.Q., 2002, Remobilization of authigenic uranium in marine sediments by bioturbation: Geochimica et Cosmochimica Acta, v. 66, p. 1759-1772, doi: 10.1016/S0016-7037(01)00886-9.

10.0 FIGURE CAPTIONS

Figure 1. Stratigraphic, depositional sequence, $\delta^{238}U$, and $\delta^{13}C_{carb}$ records of the Upper Devonian upper Devil's Gate Limestone from central Nevada with onsets of global transgressive-regressive cycles (T-R cycles of Johnson et al., 1985), and five Late Devonian extinction pulses (black triangles; McGhee, 2001). UKW and LKW refer to the upper and lower Kellwasser events. Conodont biostratigraphy by Sandberg et al. (1988, 2003). Gray shaded events D1 and D2 refer to negative $\delta^{238}U$ excursions described in text. Vertical lines with numbers 1-6 refer to recognized My-scale depositional sequences discussed in text. Curves smoothed using LOWESS smoothing procedure. Congl. = conglomerate, MST = mudstone, WK = wackestone, calc. = calcareous.

Figure 2. Cross plots of $\delta^{238}U$ against Al_{wr}, U_{wr}, Mo_{wr}, and total organic carbon (TOC). The lack of co-variation in elemental proxies for detrital input, bottom water and pore water redox conditions indicate local depositional or diagenetic conditions were not responsible for $\delta^{238}U$ trends.

Figure 3. Comparisons among Late Devonian $\delta^{238}U$ trends, extinction pulses, and contemporaneous anoxic (black), moderate or intermittently anoxic (gray), and or oxic/suboxic (white) deposits accumulating in subtropical epeiric seas, shallow-water island arc (central Asia), and accretionary complex (Thailand). The stratigraphic records of 15 Late Devonian sites were used to characterize 9 regions: western U.S., eastern and mid U.S., western Canada, southern Europe, Morocco, South China, Australia, Thailand accretionary complex, and a central Asian island

arc. Five different time intervals were defined before, during, and after the D1 and D2 negative $\delta^{238}U$ excursions and the percentage of regions accumulating anoxic to moderately anoxic sediments was utilized to generate the % anoxic seafloor plot. We define 'anoxic' seafloor as anoxic or moderately anoxic deposits occurring at that site for ≥50% of the targeted time interval. The term 'coupled' or 'decoupled' refers to a comparison between $\delta^{238}U$ trends (indicating more oxic or more reducing global seawater) and the % anoxic seafloor. The redox sediment record is compiled from: Appalachian Basin/Oklahoma (Oklahoma, Over, 2002; Tennessee, Over, 2007; New York, Bond and Wignall, 2008); Michigan (Michigan Basin, Gutschick and Sandberg, 1991; Alpena, Michigan, Over, 2002; central Michigan Basin, Formolo et al., 2014); Iowa (Day and Witzke, 2017); western Utah (Sandberg et al., 1997; Bratton et al., 1999); Nevada (this study); Section C, western Canada, Whalen et al., 2017; Germany (Steinbruch Benner section, Bond et al., 2004); France (La Serre, Montagne Noire, Feist, 1985; Bond et al., 2004); Poland (Kowala Quarry, Joachimski et al., 2002; Bond et al., 2004); Morocco (Bou Tchrafine section, Tafilalt Basin, Wendt and Belka, 1991); South China (Yangdi section, Ji, 1994; Ma et al., 2016; Nandong section, Ma and Bai, 2002); Australia (Horse Spring Range, Canning Basin, George et al., 2014), Belgium (Sinsin section, Kaiho et al., 2013), central Asian island arc (Carmichael et al., 2014), and the Thailand accretionary complex (Mai Sariang, Konigshof et al., 2012).

11.0 SUPPLEMENTARY FIGURE CAPTIONS

Figure S1. A) Late Devonian global paleogeography showing location of anoxic, intermittently to moderately anoxic, or oxic/suboxic sediment types during the late Frasnian (LKW) and F-F extinction (UKW) intervals. Note that the majority of sites are located in southern subtropical epeiric seas and mainly within the narrow Rheic Ocean. On maps, white = open ocean, light gray = shallow epeiric seas, dark gray = land. Modified from Blakey (http://deeptimemaps.com/wp-content/uploads/2016/05/380_Ma_Dev_GPT-1.png). B) Late Devonian North America (Laurentia) paleogeography showing location of study area in central Nevada with a black square (modified from Blakey http://deeptimemaps.com/wp-content/uploads/2016/05/NAM_key-375Ma_LDev.png).

Figure S2. Cross plots of $\delta^{238}U$ versus V_{wr}, Mn/Sr, Th_{carb}, weight % insoluble residue, $\delta^{13}C_{carb}$, and $\delta^{18}O_{carb}$ showing no co-variations between $\delta^{238}U$ values and proxies for detrital input, bottom water or pore water redox conditions, and burial diagenesis.

Figure S3. Comparison between $\delta^{238}U$ values and facies type (described in Table S1). Note that a wide range of $\delta^{238}U$ values are measured within a single facies type indicating $\delta^{238}U$ values are not controlled by local depositional environments or water depth. Monomict and polymict limestone conglomerate facies were not sampled because clasts and matrix were transported to studied location and may not represent redox conditions during that specific sampled time interval. Calc. = calcareous, MST = mudstone, WK = wackestone, skel. = skeletal.

Figure S4. Stratigraphic comparison among $\delta^{238}U$ trends and redox sensitive metals (RSM) in the whole rock fraction. Note that no significant enrichment of redox sensitive trace metals is observed indicating no links between local anoxic conditions and $\delta^{238}U$ values derived from the carbonate fraction.

Figure S5. Comparison between Devil's Gate, Nevada $\delta^{238}U$ and $\delta^{13}C_{carb}$ (this study) and Baisha, South China $\delta^{238}U$ and $\delta^{13}C_{carb}$ (plotted as green points, Song et al., 2017). Conodont apatite $\delta^{18}O_{apatite}$ trends from Joachimski and Buggisch (2002) showing relationships of surface seawater temperature changes (higher $\delta^{18}O$ values indicating cooler temperatures) and other proxy data. Shading and symbols the same as Figure 1.

Figure S6. Modeling results of f_{anox} (fraction of seawater U removed to anoxic facies) and anoxic seafloor area (% of total seafloor) using measured Late Devonian $\delta^{238}U$ curve.

Table S1. Facies description and depositional environment interpretations of upper Devil's Gate Limestone at the Nevada study site.

Table S2. Data table of $\delta^{238}U$, $\delta^{13}C_{carb}$, $\delta^{18}O_{carb}$, whole rock, detrital, and carbonate fraction elemental concentrations, and sample lithology.

12.0 FIGURES

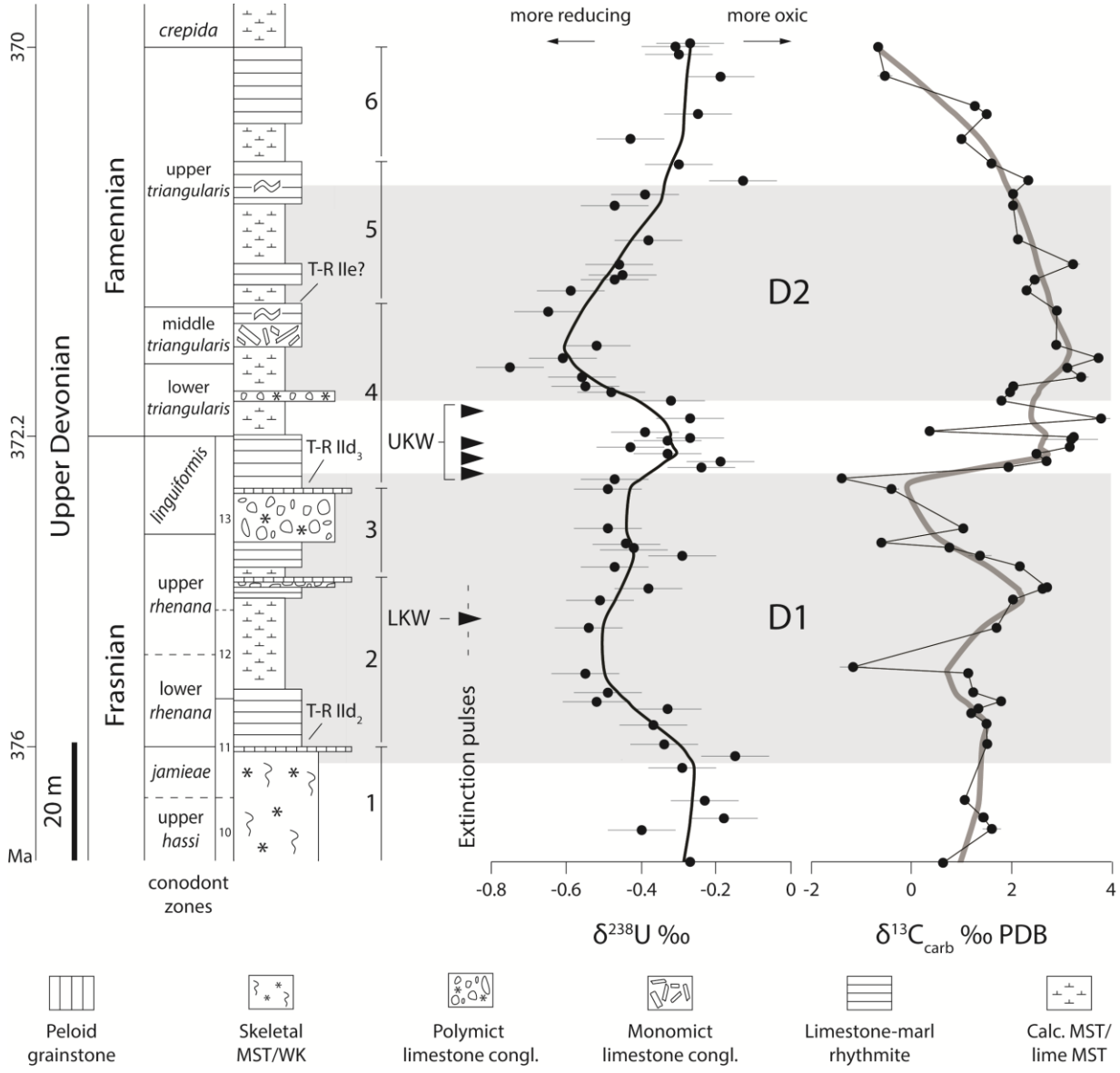

Figure 1

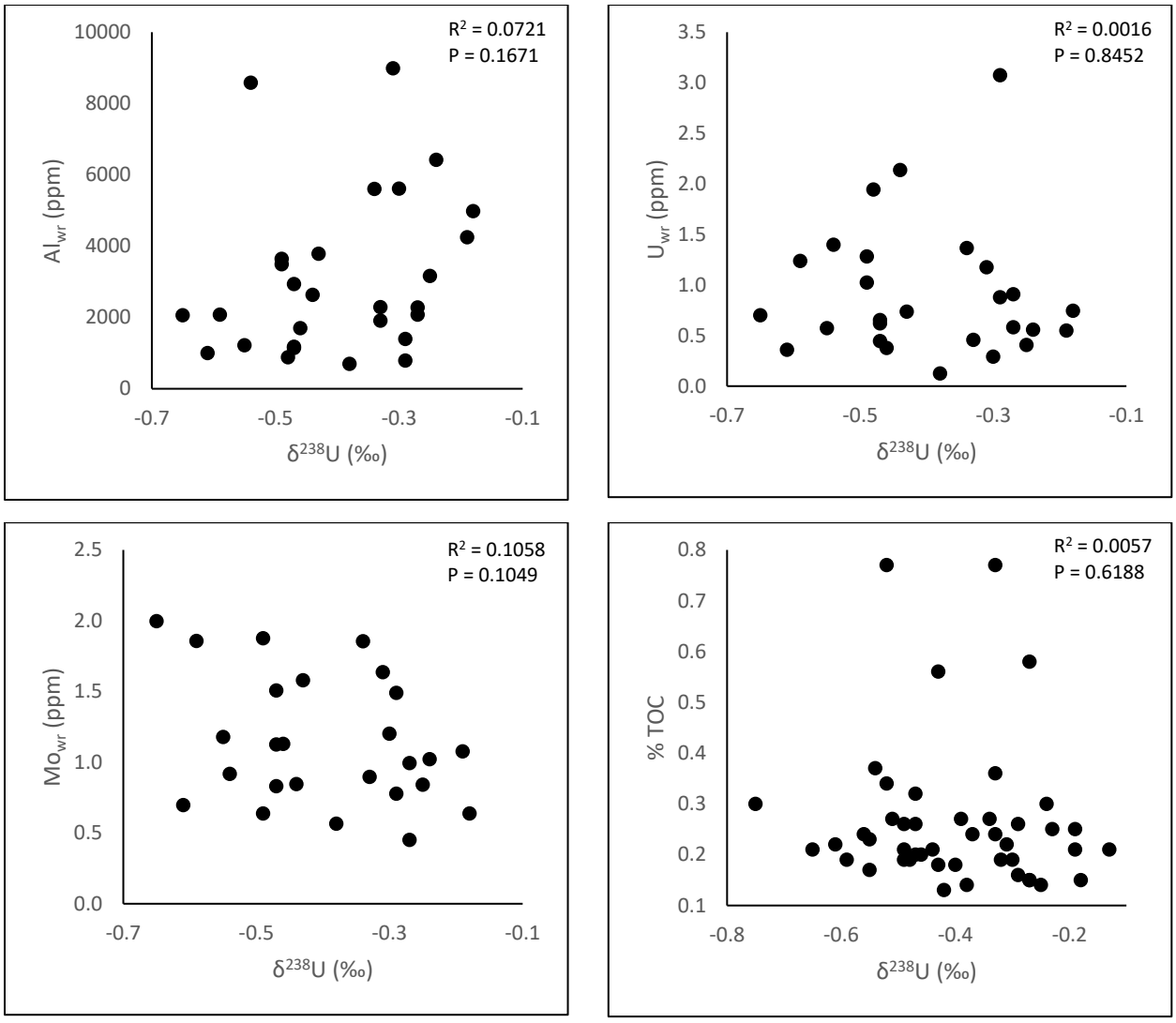
R² = 0.0721
P = 0.1671
Al_wr (ppm)
δ238U (‰)
R² = 0.0016
P = 0.8452
U_wr (ppm)
δ238U (‰)
R² = 0.1058
P = 0.1049
Mo_wr (ppm)
δ238U (‰)
R² = 0.0057
P = 0.6188
% TOC
δ238U (‰)

Figure 2

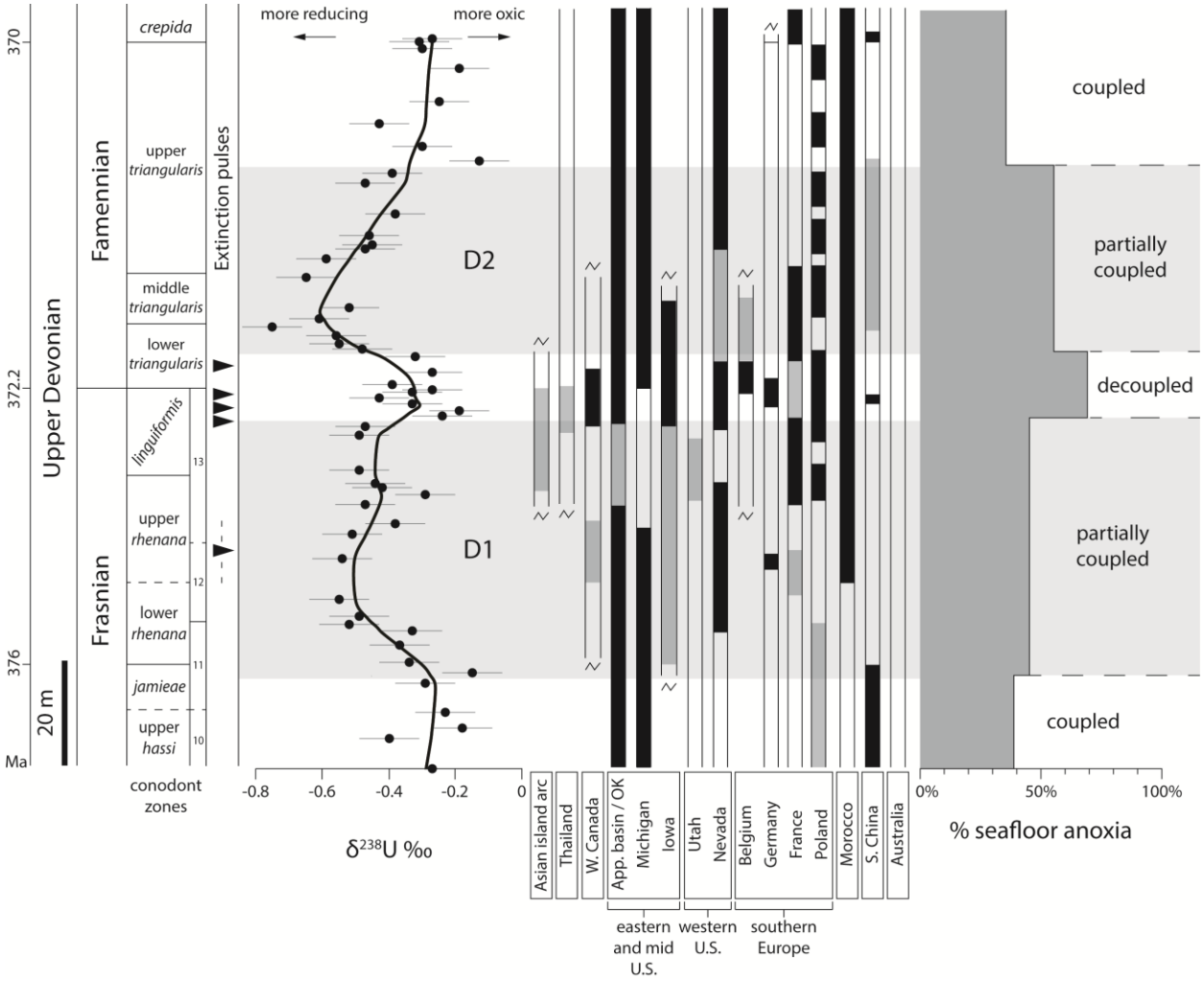
370
372.2
376
Ma
Upper Devonian
Famennian
Frasnian
20 m
crepida
upper triangularis
middle triangularis
lower triangularis
linguiformis
upper rhenana
lower rhenana
jamieae
upper hassi
13
12
11
10
conodont zones
Extinction pulses
more reducing
more oxic
D2
D1
-0.8
-0.6
-0.4
-0.2
0
δ238U ‰
Asian island arc
Thailand
W. Canada
App. basin / OK
Michigan
Iowa
Utah
Nevada
Belgium
Germany
France
Poland
Morocco
S. China
Australia
eastern and mid U.S.
western U.S.
southern Europe
coupled
partially coupled
decoupled
partially coupled
coupled
0%
50%
100%
% seafloor anoxia

Figure 3

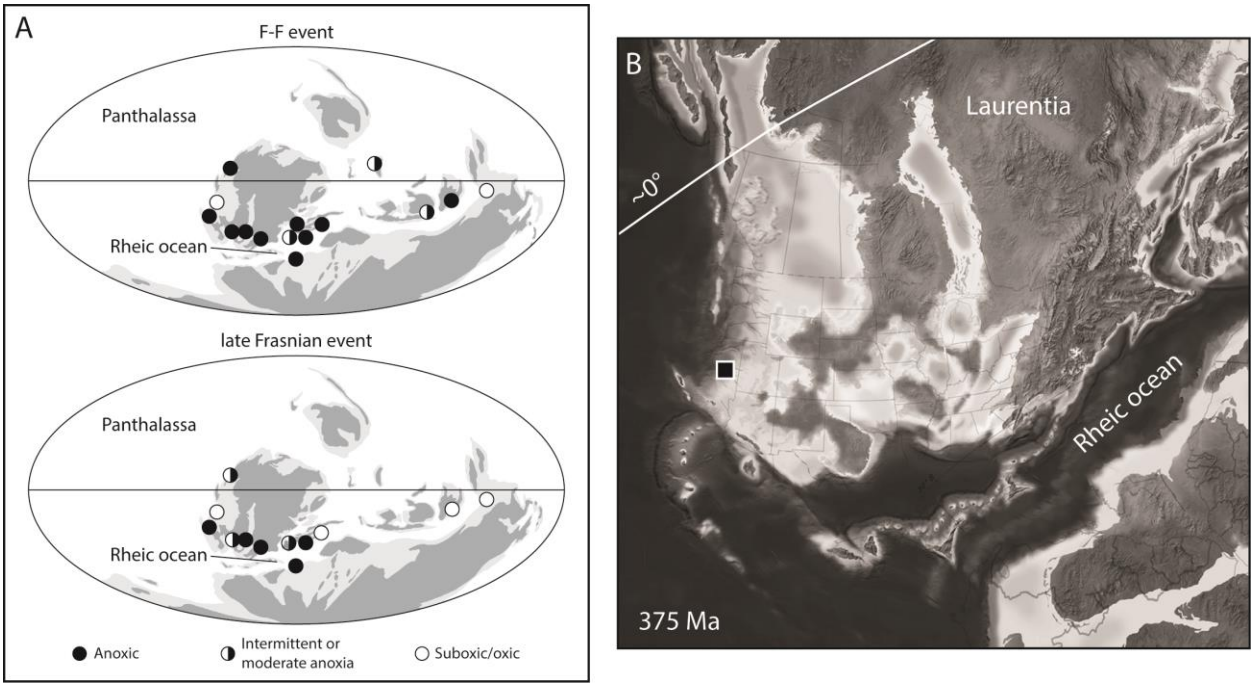
A
F-F event
Panthalassa
Rheic ocean
late Frasnian event
Panthalassa
Rheic ocean
Anoxic
Intermittent or moderate anoxia
Suboxic/oxic
B
Laurentia
~0°
Rheic ocean
375 Ma

Figure S1

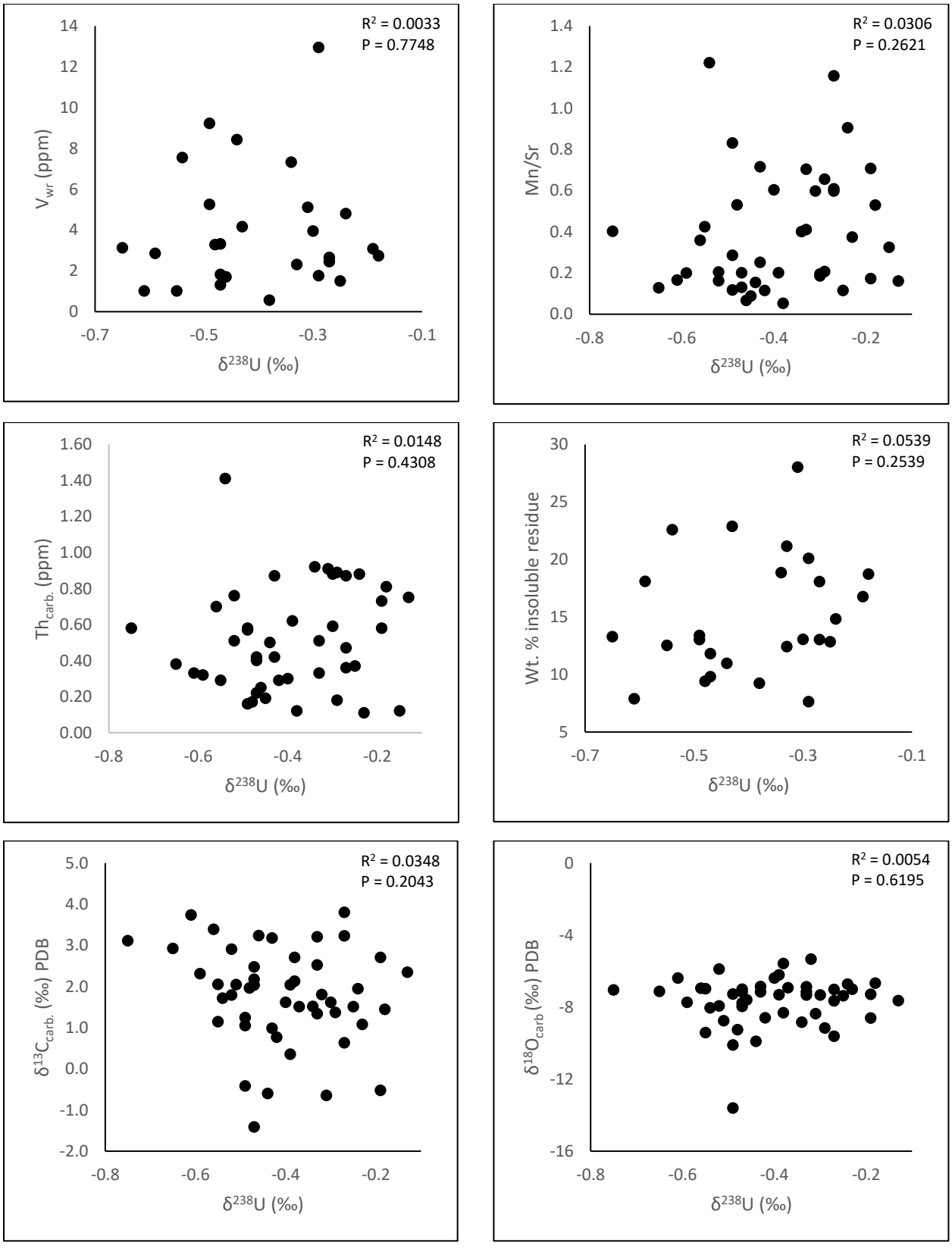
R² = 0.0033
P = 0.7748
V_wr (ppm)
δ²³⁸U (‰)
R² = 0.0306
P = 0.2621
Mn/Sr
δ²³⁸U (‰)
R² = 0.0148
P = 0.4308
Th_carb. (ppm)
δ²³⁸U (‰)
R² = 0.0539
P = 0.2539
Wt. % insoluble residue
δ²³⁸U (‰)
R² = 0.0348
P = 0.2043
δ¹³C_carb. (‰) PDB
δ²³⁸U (‰)
R² = 0.0054
P = 0.6195
δ¹⁸O_carb (‰) PDB
δ²³⁸U (‰)

Figure S2

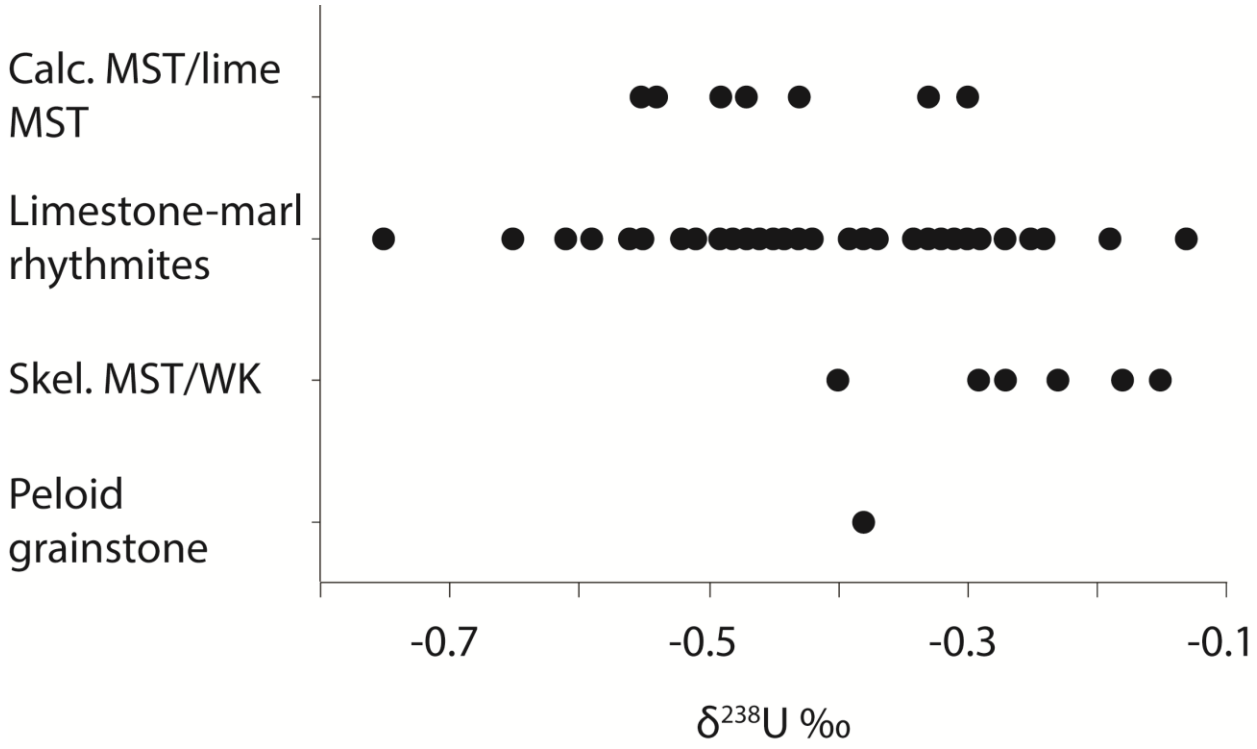
Calc. MST/lime MST
Limestone-marl rhythmites
Skel. MST/WK
Peloid grainstone
-0.7
-0.5
-0.3
-0.1
δ238U ‰

Figure S3

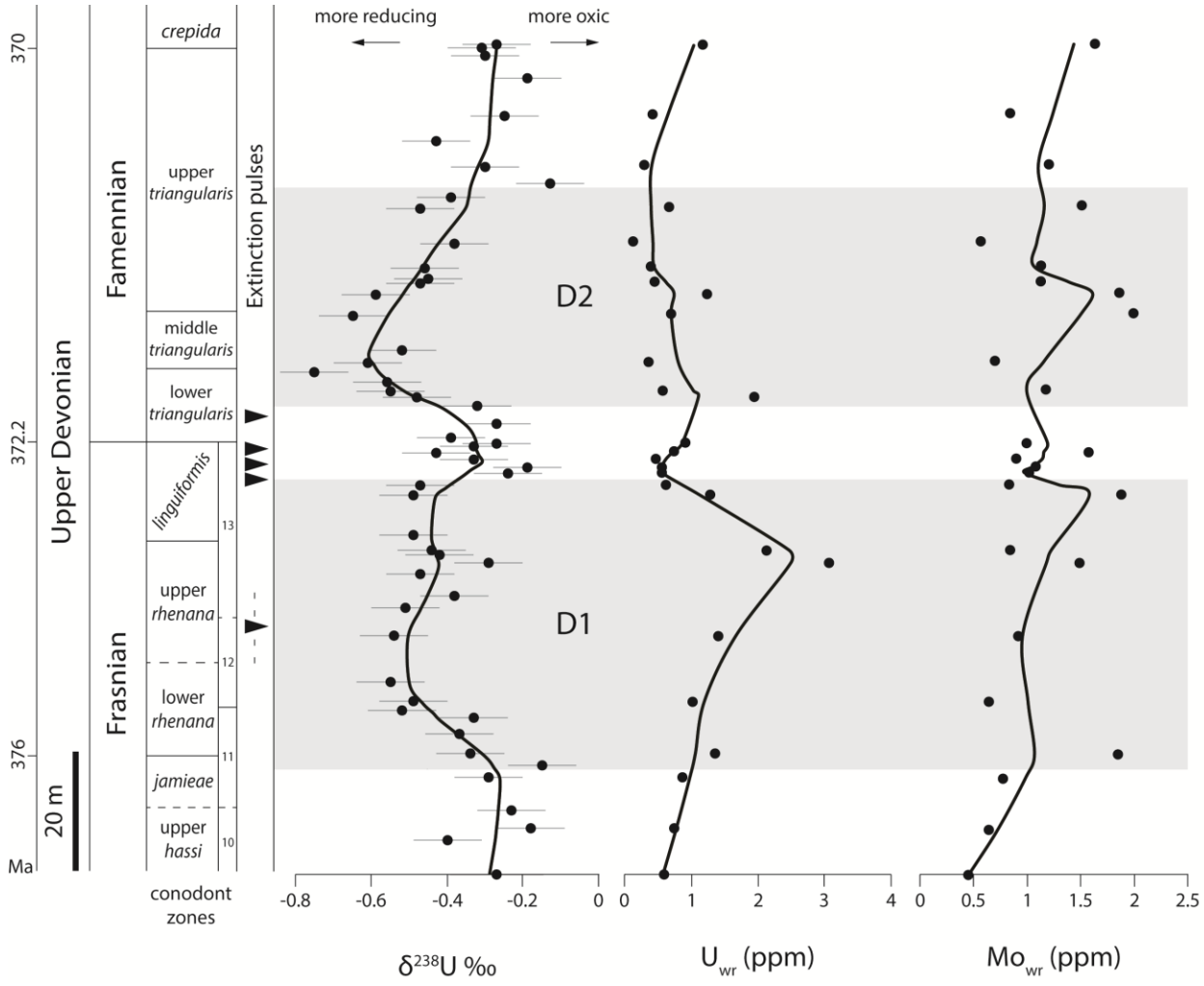
more reducing
more oxic
370
372.2
376
Ma
Upper Devonian
Famennian
Frasnian
20 m
crepida
upper triangularis
middle triangularis
lower triangularis
linguiformis
upper rhenana
lower rhenana
jamieae
upper hassi
13
12
11
10
conodont zones
Extinction pulses
D2
D1
-0.8
-0.6
-0.4
-0.2
0
δ238U ‰
0
1
2
3
4
Uwr (ppm)
0
0.5
1
1.5
2
2.5
Mowr (ppm)

Figure S4

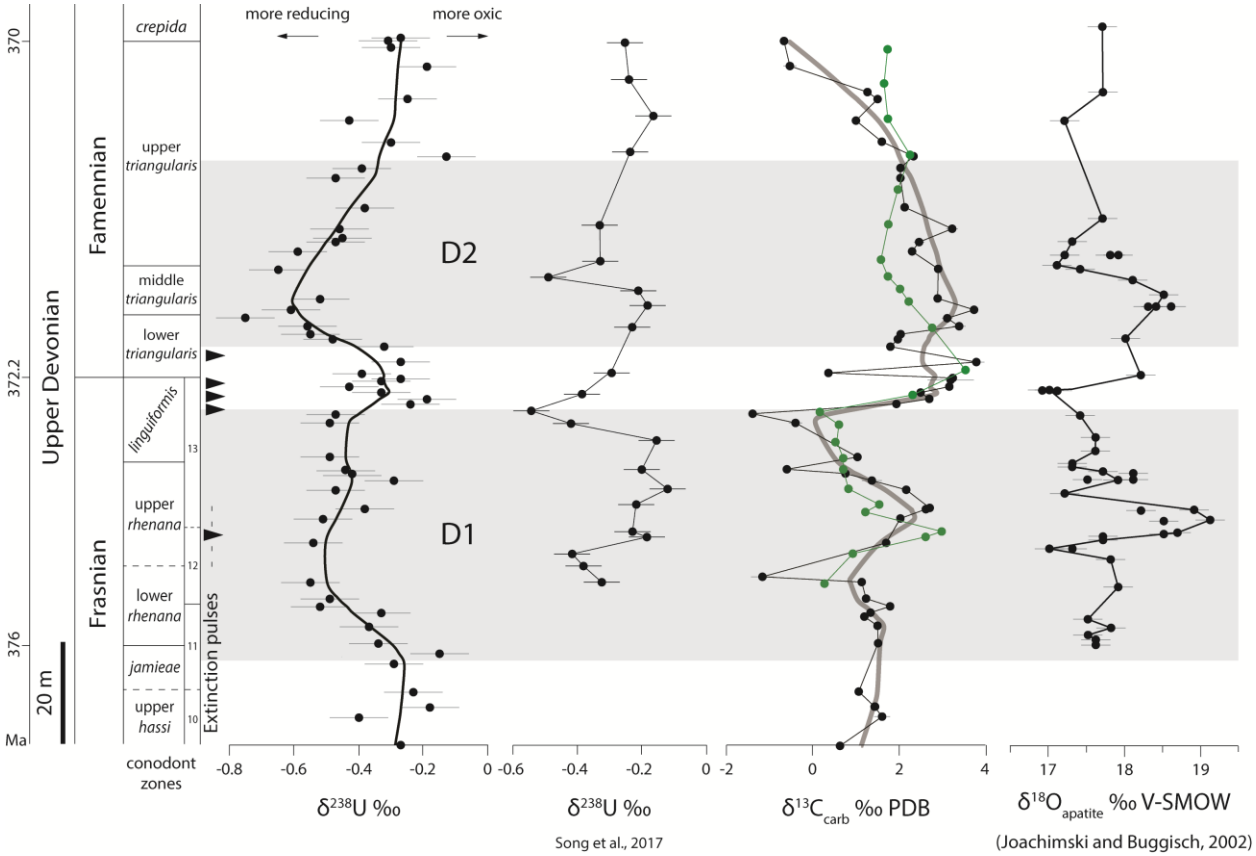
more reducing
more oxic
crepida
upper triangularis
middle triangularis
lower triangularis
linguiformis
upper rhenana
lower rhenana
jamieae
upper hassi
Famennian
Frasnian
Upper Devonian
370
372.2
376
Ma
20 m
13
12
11
10
Extinction pulses
D2
D1
conodont zones
-0.8 -0.6 -0.4 -0.2 0
δ238U ‰
-0.6 -0.4 -0.2 0
δ238U ‰
Song et al., 2017
-2 0 2 4
δ13Ccarb ‰ PDB
17 18 19
δ18Oapatite ‰ V-SMOW
(Joachimski and Buggisch, 2002)

Figure S5

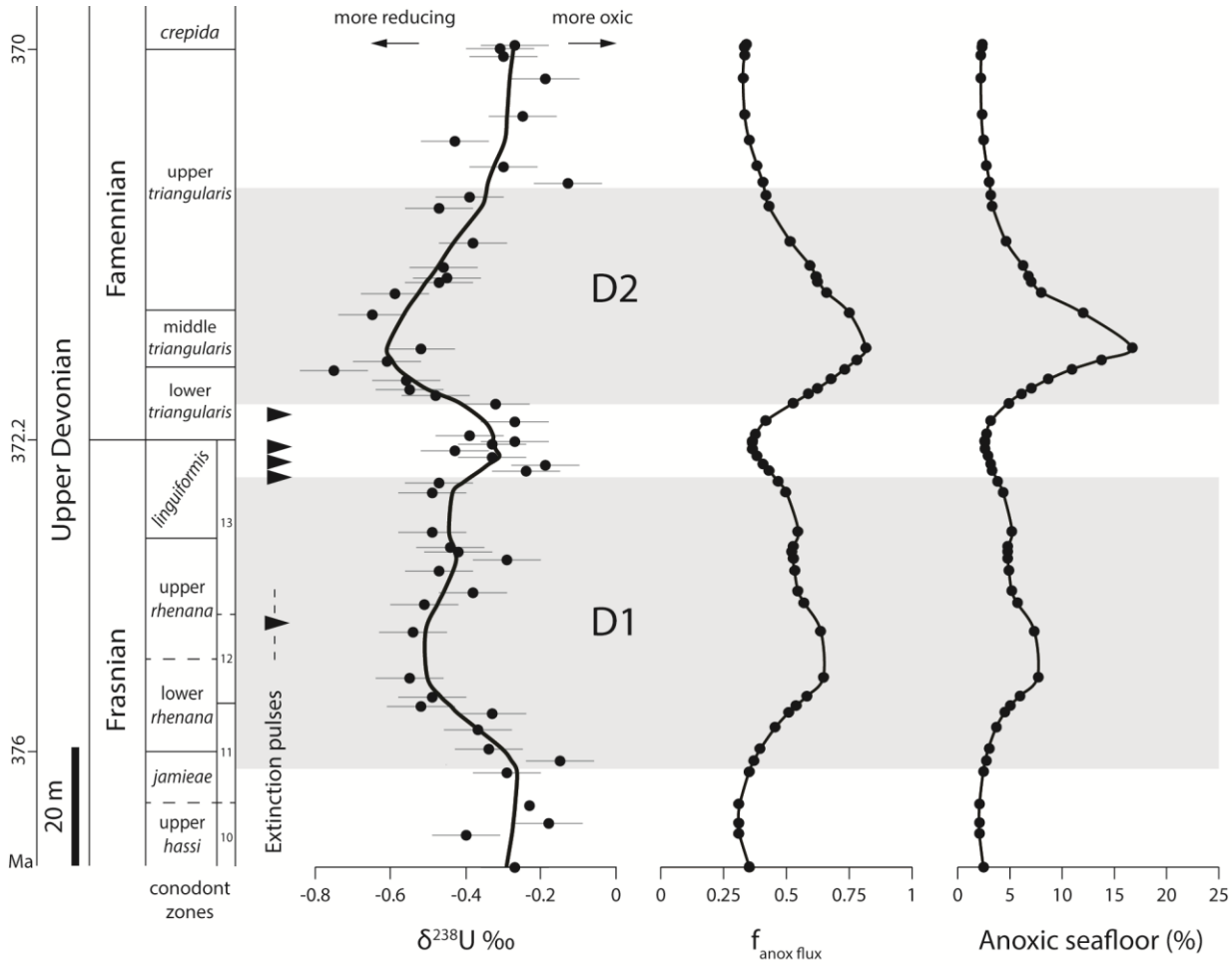
370
372.2
376
Ma
Upper Devonian
20 m
Famennian
Frasnian
crepida
upper triangularis
middle triangularis
lower triangularis
linguiformis
upper rhenana
lower rhenana
jamieae
upper hassi
13
12
11
10
conodont zones
Extinction pulses
more reducing
more oxic
D2
D1
-0.8
-0.6
-0.4
-0.2
0
δ238U ‰
0
0.25
0.5
0.75
1
f anox flux
0
5
10
15
20
25
Anoxic seafloor (%)

Figure S6

13.0 TABLES

Table S1. Facies description and depositional environment interpretations of upper Devil's Gate Limestone at the study site.

Facies	Lithology	Sedimentary structures	Biota	Depositional environment
Peloid grainstone	Grainstone	Planar mechanical laminations	Barren	High-energy shallow subtidal (oxic)
Skeletal mudstone/ wackestone	Mudstone/ wackestone	Massive	Sparse rugose coral, crinoids, brachiopods, gastropods, skeletal fragments, well bioturbated	Shallow subtidal (oxic)
Polymict limestone conglomerate	Matrix- to clast-supported limestone conglomerate. Clasts composed of massive lime MST to argillaceous lime MST	Massive lenticular beds, moderately rounded, pebble to cobble-size clasts	Sparse skeletal fragments in matrix and clasts including rugose coral, brachiopods, gastropods, rare nautiloid	Debris flow deposits Intermediate to deep subtidal (suboxic)
Monomict limestone conglomerate	Matrix- to clast-supported limestone conglomerate. Clasts composed of laminated to massive lime MST/WK, matrix composed of lime MST to argillaceous lime MST	Massive lenticular beds, moderately rounded pebble- to cobble-size clasts	Fine skeletal debris in clasts and matrix, occasional bioturbation	Debris flow deposits deep subtidal (suboxic to anoxic)
Limestone-marl rhythmites	Lime mudstone interbedded with argillaceous lime mudstone (marl)	Even to nodular bedded, both layers contain common suspension laminae, sparse graded layers, common syndepositional folding, rare flame structures	Rare fine skeletal debris, occasional bioturbation	Deep subtidal (suboxic to anoxic)
Calcareous mudstone w/interbedded lime mudstone	Calcareous (terrigenous) mudstone with sparse interbedded lime MST	Suspension laminae in both layers	Barren	Deepest subtidal (anoxic)

Table S2. Data table of $\delta^{238}U$, $\delta^{13}C_{carb}$, $\delta^{18}O$, whole rock, detrital, and carbonate fraction elemental concentrations, and sample lithology.

Sample	Meter	δ238U	2SD	δ13C	δ18O	U_{wr} (ppm)	Mo_{wr} (ppm)	V_{wr} (ppm)	Al_{wr} (ppm)	% insol.	Th_{carb}	%TOC	$U_{carb.}$ (ppm)	$Mo_{carb.}$ (ppm)	$V_{carb.}$ (ppm)	Mg/Ca	Mn/Sr	Lithology
DVG 0	0	-0.27	0.12	0.63	-9.61	0.58	0.45	2.66	2081	13	0.36	0.15	0.39	-	1.76	0.006	1.16	micrite/wacke
DVG 5.5	5.5	-0.4	0.10	1.62	-6.38	-	-	-	-	-	0.30	0.18	0.36	0.01	1.01	0.007	0.60	micrite/wacke
DVG 7.5	7.5	-0.18	0.10	1.45	-6.66	0.74	0.64	2.74	4978	19	0.81	0.15	0.36	0.00	1.32	0.022	0.53	micrite/wacke
DVG 10.5	10.5	-0.23	0.03	1.08	-7.01	-	-	-	-	-	0.11	0.25	0.44	0.01	1.67	0.007	0.37	micrite/wacke
DVG 16	16	-0.29	0.10	-	-	0.88	0.78	1.77	793	8	0.18	0.16	0.68	0.04	1.25	0.008	0.66	micrite/wacke
DVG 18	18	-0.15	0.09	-	-	-	-	-	-	-	0.12	-	0.37	-	1.15	0.005	0.33	micrite/wacke
DVG 20	20	-0.34	0.08	1.52	-8.84	1.37	1.85	7.33	5606	19	0.92	0.27	0.78	-	1.59	0.009	0.40	micrite
DVG 23.5	23.5	-0.37	0.08	1.51	-6.92	-	-	-	-	-	-	0.24	-	-	-	-	-	micrite
DVG 25.3	25.3	-	-	1.21	-7.54	0.77	0.49	3.04	2160	10	0.34	0.21	-	-	-	-	-	micrite
DVG 26	26	-0.33	0.07	1.34	-7.15	-	-	-	-	-	-	0.24	-	-	-	-	-	micrite
DVG 27.2	27.2	-0.52	0.14	1.79	-7.94	-	-	-	-	-	0.76	0.34	0.66	0.03	0.66	0.009	0.20	micrite
DVG 28.8	28.8	-0.49	0.11	1.24	-13.6	1.02	0.64	9.23	3648	13	0.58	0.19	0.58	-	4.28	0.006	0.83	micrite
DVG 32	32	-0.55	0.02	1.14	-6.98	-	-	-	-	-	-	0.23	-	-	-	-	-	micrite
DVG 33	33	-	-	-1.17	-7.18	-	-	-	-	-	-	0.30	-	-	-	-	-	micrite
DVG 39.8	39.8	-0.54	0.05	1.72	-8.05	1.40	0.92	7.55	8584	23	1.41	0.37	0.41	0.13	1.21	0.068	1.22	micrite
DVG 44.5	44.5	-0.51	0.07	2.05	-8.76	-	-	-	-	-	-	0.27	-	-	-	-	-	micrite
DVG 46.3	46.3	-	-	2.64	-7.53	-	-	-	-	-	-	0.13	-	-	-	-	-	grainstone
DVG 46.5	46.5	-0.38	0.12	2.71	-8.31	-	-	-	-	-	-	-	-	-	-	-	-	grainstone
DVG 50.1	50.1	-0.47	0.05	2.18	-7.15	-	-	-	-	-	-	0.32	-	-	-	-	-	micrite
DVG 52	52	-0.29	0.04	1.37	-9.16	3.08	1.49	12.95	1396	20	0.89	0.26	1.71	0.02	4.15	0.009	0.21	micrite
DVG 53.3	53.3	-0.42	0.08	0.77	-8.59	-	-	-	-	-	0.29	0.13	0.62	-	1.71	0.009	0.12	micrite
DVG 54.1	54.1	-0.44	0.01	-0.60	-9.90	2.14	0.84	8.43	2631	11	0.50	0.21	1.52	0.05	4.01	0.012	0.15	micrite
DVG 56.7	56.7	-0.49	0.06	1.05	-10.10	-	-	-	-	-	0.16	0.21	0.24	0.00	3.70	0.006	0.12	micrite
EDG 1.3	63.3	-0.49	0.05	-0.41	-7.28	1.28	1.87	5.26	3496	13	0.57	0.26	0.76	0.18	2.35	0.012	0.29	micrite
EDG 3	65	-0.47	0.10	-1.41	-7.00	0.62	0.83	1.31	1175	12	0.42	0.26	0.40	0.06	0.67	0.010	0.13	micrite

Sample	Meter	δ238U	2SD	δ13C	δ18O	U_{wr} (ppm)	Mo_{wr} (ppm)	V_{wr} (ppm)	Al_{wr} (ppm)	% insol.	Th_{carb}	%TOC	$U_{carb.}$ (ppm)	$Mo_{carb.}$ (ppm)	$V_{carb.}$ (ppm)	Mg/Ca	Mn/Sr	Lithology
EDG 5	67	-0.24	0.02	1.94	-6.72	0.56	1.02	4.81	6423	15	0.88	0.30	0.20	0.01	0.72	0.026	0.91	micrite
EDG 6	68	-0.19	0.05	2.71	-7.29	0.55	1.08	3.08	4251	17	0.73	0.25	0.27	0.03	0.58	0.017	0.71	micrite
EDG 7.3	69.3	-0.33	0.05	2.52	-6.87	0.46	0.90	2.31	2289	12	0.51	0.36	0.26	-	0.68	0.016	0.70	micrite
EDG 8.5	70.5	-0.43	0.12	3.18	-7.15	0.74	1.58	4.17	3791	23	0.87	0.56	0.52	0.04	0.85	0.017	0.72	micrite
EDG 9.6	71.6	-0.33	0.07	3.21	-7.33	-	-	-	1909	21	0.33	0.77	0.46	0.03	0.57	0.007	0.41	micrite
EDG 10	72	-0.27	0.04	3.23	-7.01	0.91	0.99	2.45	2277	18	0.47	0.58	0.74	0.05	0.68	0.008	0.61	micrite
DVG 73	73	-0.39	0.04	0.36	-6.21	-	-	-	-	-	-	-	-	-	-	-	-	micrite
DVG 75.3	75.3	-0.27	0.08	3.80	-7.65	-	-	-	-	-	-	0.15	-	-	-	-	-	micrite
EDG 16.3	78.3	-0.32	0.06	1.80	-5.34	-	-	-	-	-	-	0.19	-	-	-	-	-	micrite
EDG 17.8	79.8	-0.48	0.10	1.96	-9.26	1.95	-	3.28	881	9	0.17	0.19	1.44	0.04	1.08	0.006	0.53	micrite
EDG 18.8	80.8	-0.55	0.03	2.05	-9.41	0.57	1.18	1.02	1220	13	0.29	0.17	0.51	0.05	0.61	0.008	0.43	micrite
EDG 20.3	82.3	-0.56	0.06	3.39	-6.96	-	-	-	-	-	0.70	0.24	0.23	0.30	0.65	0.013	0.36	micrite
EDG 22	84	-0.75	0.04	3.11	-7.05	-	-	-	-	-	0.58	0.30	0.50	0.07	1.35	0.021	0.40	micrite
EDG 23.6	85.6	-0.61	0.01	3.74	-6.38	0.36	0.70	1.02	999	8	0.33	0.22	0.26	0.13	0.49	0.013	0.17	micrite
EDG 25.7	87.7	-0.52	0.03	2.91	-5.89	-	-	-	-	-	0.51	0.77	0.28	0.26	0.82	0.018	0.16	micrite
EDG 31.5	93.5	-0.65	0.01	2.92	-7.12	0.70	1.99	3.14	2061	13	0.38	0.21	0.42	0.08	0.92	0.011	0.13	micrite
EDG 35	97	-0.59	0.08	2.31	-7.74	1.24	1.85	2.86	2078	18	0.32	0.19	0.87	0.13	1.01	0.009	0.20	micrite
EDG 36.9	98.9	-0.47	0.11	2.48	-7.77	0.44	1.12	1.83	1148	-	0.22	-	-	-	-	-	-	micrite
EDG 37.7	99.7	-0.45	0.05	-	-	-	-	-	-	-	0.19	-	0.31	0.09	0.71	0.008	0.09	micrite
EDG 39.5	101.5	-0.46	0.04	3.24	-7.60	0.38	1.13	1.71	1696	-	0.25	0.20	0.20	0.05	0.54	0.010	0.07	micrite
EDG 43.6	105.6	-0.38	0.10	2.13	-5.58	0.13	0.57	0.57	694	9	0.12	0.14	0.08	0.01	0.20	0.010	0.05	micrite
EDG 49.5	111.5	-0.47	0.09	2.04	-7.96	0.65	1.51	3.32	2939	10	0.40	0.20	0.40	0.14	1.19	0.008	0.20	micrite
EDG 51.4	113.4	-0.39	0.03	2.04	-7.32	-	-	-	-	-	0.62	0.27	0.22	0.66	0.96	0.013	0.20	micrite
EDG 53.7	115.7	-0.13	0.08	2.35	-7.64	-	-	-	-	-	0.75	0.21	0.32	0.06	0.95	0.015	0.16	micrite
EDG 56.5	118.5	-0.3	0.05	1.62	-7.32	0.29	1.20	3.95	5615	13	0.88	0.19	0.17	0.47	1.18	0.025	0.20	micrite
EDG 60.8	122.8	-0.43	0.05	0.99	-6.85	-	-	-	-	-	0.42	0.18	0.16	0.00	0.70	0.007	0.25	micrite
EDG 65	127	-0.25	0.09	1.51	-7.36	0.41	0.84	1.51	3162	13	0.37	0.14	0.21	0.01	0.61	0.009	0.12	micrite
EDG 66.3	128.3	-	-	1.28	-7.50	-	-	-	-	-	0.48	0.14	-	-	-	-	-	micrite
EDG 71.3	133.3	-0.19	0.06	-0.52	-8.60	-	-	-	-	-	0.58	0.21	0.74	0.16	2.13	0.015	0.17	micrite

Sample	Meter	δ238U	2SD	δ13C	δ18O	U_{wr} (ppm)	Mo_{wr} (ppm)	V_{wr} (ppm)	Al_{wr} (ppm)	% insol.	Th_{carb}	%TOC	$U_{carb.}$ (ppm)	$Mo_{carb.}$ (ppm)	$V_{carb.}$ (ppm)	Mg/Ca	Mn/Sr	Lithology
EDG 75.1	137.1	-0.30	0.04	-	-	-	-	-	-	-	0.59	-	0.37	0.04	1.31	0.018	0.19	micrite
EDG 76.5	138.5	-0.31	0.07	-0.65	-8.36	1.18	1.63	5.11	8986	28	0.91	0.22	0.68	0.10	1.09	0.029	0.60	micrite
EDG 77	139	-0.27	0.07	-	-	-	-	-	-	-	0.87	-	0.67	0.09	1.02	0.029	0.60	micrite
Matrix	18	-0.13	0.09	-	-	-	-	-	-	-	-	-	-	-	-	-	-	micrite/wacke
Rugose	18	-0.25	0.02	-	-	-	-	-	-	-	-	-	-	-	-	-	-	micrite/wacke